Sorption-Enhanced Variable Volume Batch-Membrane Steam Methane Reforming at Low Temperature: Experimental Demonstration and Kinetic Modeling

David M. Anderson[1], Mohamed H. Nasr[1], Thomas M. Yun[1], Peter A. Kottke[1] and Andrei G. Fedorov[1,2,*]

1. G.W. Woodruff School of Mechanical Engineering, Georgia Institute of Technology, Atlanta Georgia, 30332, United States
2. Parker H. Petit Institute of Bioengineering and Bioscience, Georgia Institute of Technology, Atlanta Georgia, 30332, United States

*corresponding author: AGF@gatech.edu

S1. Introduction

This document contains supplementary information supporting the experimental results reported in the main body of the paper, as well as additional detail on the kinetic models used to determine reaction rates, adsorption rates and perform the timescale analysis.

S2. Experimental Apparatus

The P&ID of the experimental apparatus, included in the main paper, is shown again for reference:

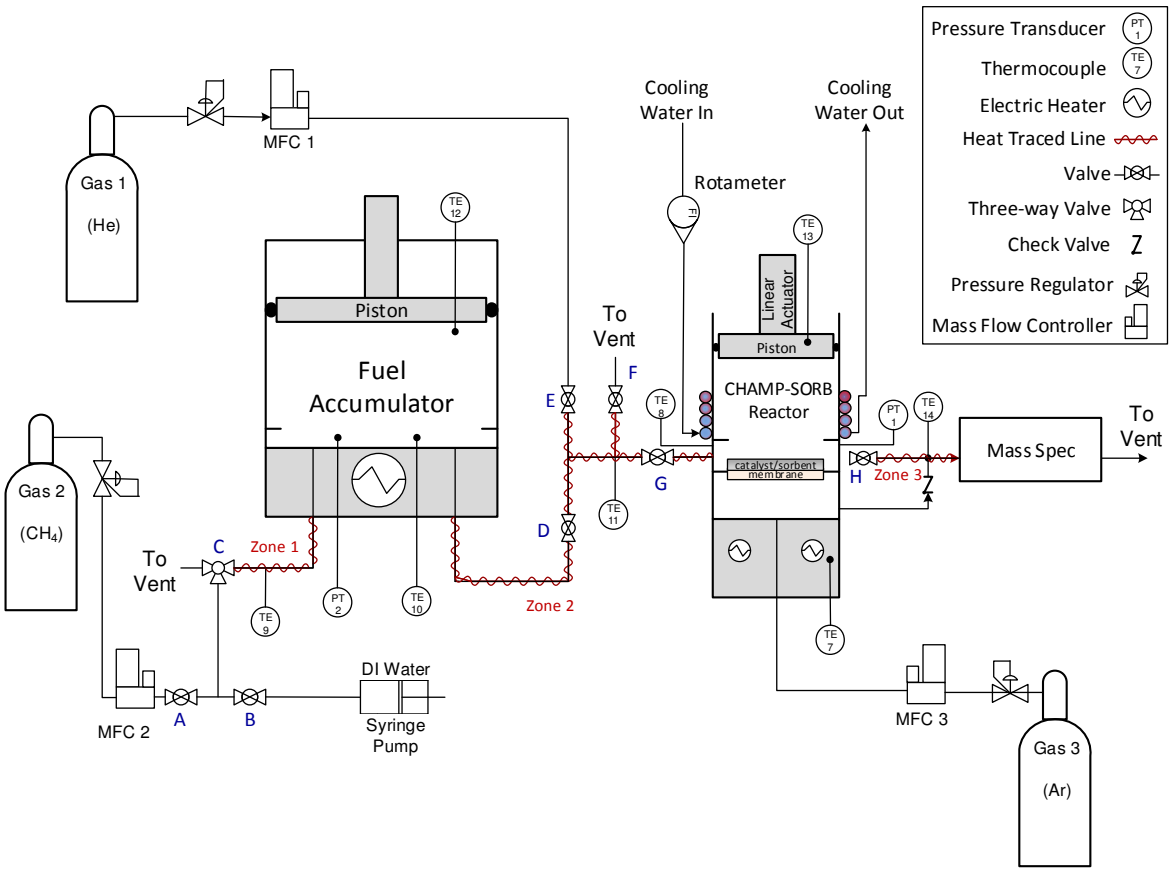

Figure S1: P&ID of CHAMP-SORB experimental testbed. The piping in zones 1-3 is insulated and heated with NiCr resistance heaters to ensure any steam content remains superheated.

Figure S2 contains a picture of the experimental apparatus, with the physical parts labeled to show their correspondence to items on the P&ID.

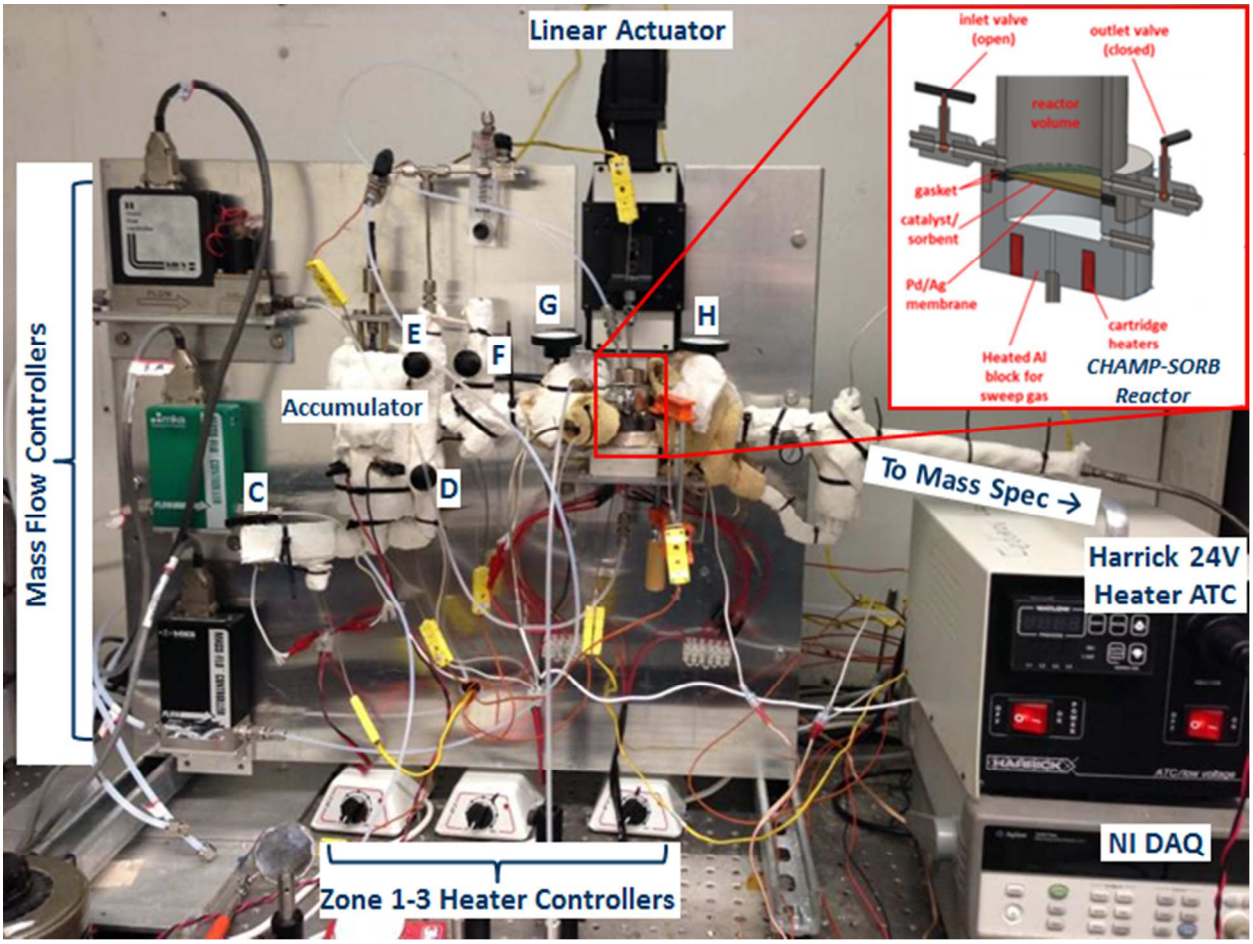

Figure S2: Experimental CHAMP-SORB testbed apparatus

The fuel accumulator, designed to hold and deliver a CH_4/steam mixture at the desired S/C ratio, and the CHAMP-SORB reactor were both constructed in a piston/cylinder arrangement out of 17-4 stainless steel. Because the reactor and accumulator are of a comparable volume to their inlet and outlet valves, the ratio of working volume (*i.e.* volume that can be swept by piston motion), to dead volume (*i.e.* the volume occupied by valves, piping, etc.) must be considered. Figure S3 presents experimental data used to determine the dead volume of the testbed CHAMP-SORB reactor. The piston was moved via the linear actuator between its maximum and minimum displacement positions twice, and the pressure and temperature were continually recorded using a custom-written LabVIEW data acquisition program.

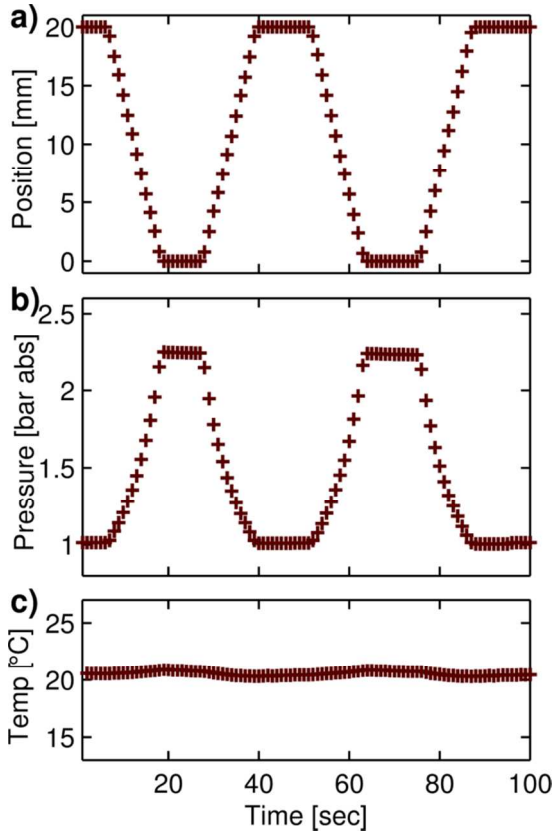

Figure S3: Experimental data for calculation of CHAMP-SORB testbed reactor dead volume

As the reactor volume was compressed, the pressure increased and temperature remained nearly constant (less than 0.1% deviation between the maximum and minimum recorded values in absolute temperature). Assuming that the system is closed (*i.e.* no moles of gas escape from the reactor), the theoretical relationship between pressure and volume for an isothermal control volume can be determined using the ideal gas equation of state:

$$NR_uT = PV = constant \quad \text{(S1)}$$

Using the known cross-sectional area of the reactor, the maximum volume occupied by the gas mixture can be expressed as $V_{max} = V_d + A_c\Delta x$, where the dead volume (V_d) is the volume of the

reactor when the piston is at its minimum position and Δx is the distance spanned by the piston as it moves from its minimum to maximum displacement. As such, from eq S1 it follows that:

$$V_d = \left(\frac{P_{min}}{P_{max} - P_{min}}\right) A_c \Delta x \qquad \text{(S2)}$$

where P_{min} is the reactor pressure at maximum volume and P_{max} is the reactor pressure at minimum volume. Using the experimental data from Figure S3a, the maximum and dead volumes of the reactor were calculated to be 8.79 cm^3 and 3.97 cm^3, respectively. To verify the accuracy of this calculation, all the pressure and position data points from Figure S3a are plotted against one another on Figure S4 and compared to the predicted change in pressure by the ideal gas equation of state. The accumulator's maximum and minimum volumes were assessed using a similar technique and calculated to be 122.8 cm^3 and 36.3 cm^3, respectively.

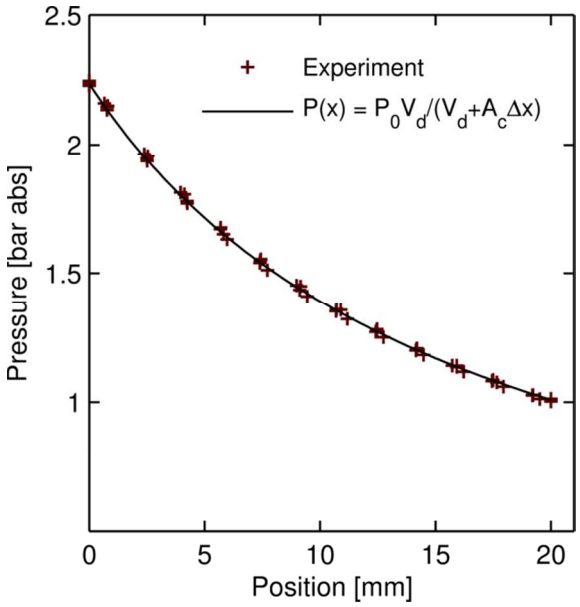

Figure S4: Relationship between position and pressure as measured experimentally vs. predicted by the ideal gas equation of state

Temperature and pressure were monitored in the locations indicated on the P&ID using K-type thermocouples (Omega Technologies) and high temperature miniature pressure transducers (Kulite Semiconductor Products). These probes were connected to an Agilent 34970A data acquisition/switch unit (DAQ) interfacing with a custom LabVIEW program to record temperature and pressure. Additionally, a NLS4-series linear actuator and a NSC-A1 stepper motor (Newmark Systems) were integrated in LabVIEW with closed-loop PID control to the reactor piston position. Effluent from the reactor was carried to a mass spectrometer (Hiden Analytical, HPR-20) for analysis using a sweep argon gas stream metered by mass flow controllers (MKS Instruments, 1179A series) with a precision of +/-1% of full scale.

The accumulator, CHAMP-SORB reactor and all lines/valves in between were thermally insulated using ceramic fiber insulation (Refractory Specialties Incorporated) and heated by electric resistance heaters (Omega Technologies and Sun Electric Heater Company) to avoid condensation in any parts of the test loop. The membrane and catalyst/sorbent layer were heated to 400°C, controlled by a Harrick 24V automatic temperature controller. The piston of the CHAMP-SORB reactor was sealed against the cylinder bore using a perfluoroelastomer o-ring rated to a maximum temperature of 330°C, necessitating the use of cooling water metered through a rotameter (Cole-Palmer) at 1 gallon/hr flowing through stainless steel tubing wrapped around the reactor cylinder to preserve the seal. The interface between the piston o-ring and the reactor cylinder wall was lubricated using high temperature Krytox XHT-1000 perfluoropolyether oil (DuPont).

S3. Experimental Methods

S3.1 Mass Spectrometer Calibration

To calculate the flowrate of an effluent from the CHAMP-SORB reactor, the mass spectrometer (MS) in Figure S1 was used in conjunction with an argon sweep gas at a known flowrate metered by a mass

flow controller (MFC). Prior to conducting a reactor experiment, a gas mixture consisting of metered flows of both Ar and each expected analyte was sent to the MS for detection. The ratio of these flowrates was modified periodically by adjusting the MFC settings, creating a set of data for known MFC flow ratios and corresponding MS measurements. The raw data for a H_2 MS calibration run is presented in Figure S5.

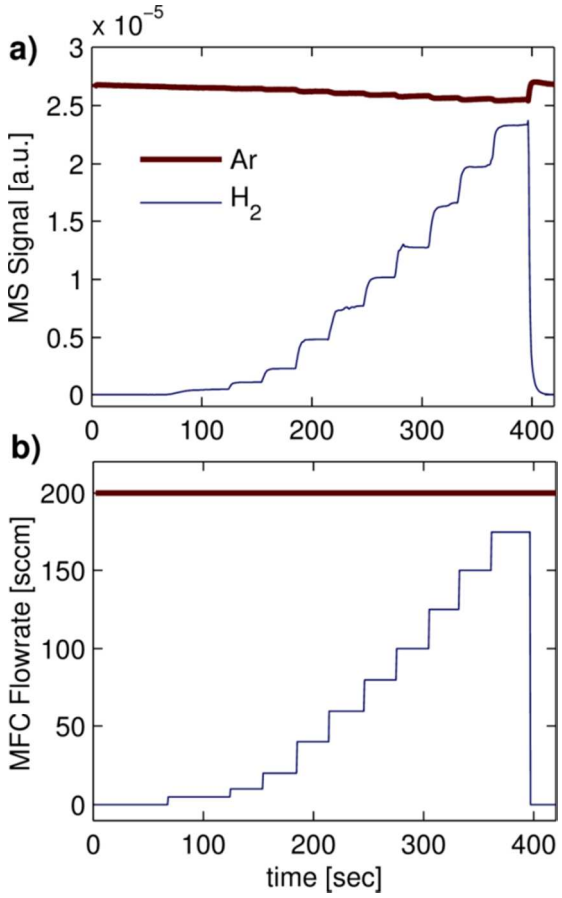

Figure S5 Raw experimental data for H_2 used in mass spectrometer calibration

The reported H_2 signal in Figure S5a is the increase in MS signal from a baseline reading of the H_2 signal when pure Ar gas was sent to the MS (although two orders of magnitude less than the Ar signal, this detected value is non-zero). Similarly, when utilizing experimental MS data to calculate the flowrate of any other analyte species, the MS signal of each analyte is also first adjusted to be relative to the analyte signal detected when pure sweep (Ar) gas is flowing to the spectrometer. This process accounts

for baseline removal due to any small drift that may occur during the experimental process, and allows the least squares fitted line representing the MFC to MS ratio to pass through the origin.

During a calibration experiment, at each flow ratio the gas mixture was sent to the mass spectrometer for a minimum of 30 seconds. The ratio of the measured H_2 to Ar MS signal is extracted from the data by averaging over the final (stable) 15 seconds of data prior to switching to the next MFC flowrate ratio. The relationship between analyte to sweep gas MFC (known) flowrate ratio to MS signal ratio is reported in Figure S6.

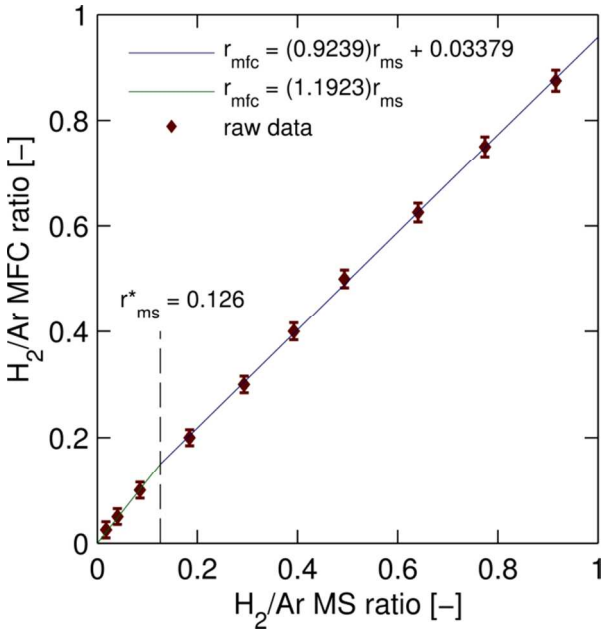

Figure S6: Metered H_2 to Ar MFC flowrate ratio vs. measured MS signal ratio. Least squares linear regression relating the two parameters is used in determining analyte flowrate during CHAMP-SORB experiments from MS data (the transition between segments of the piecewise fitted curve is marked with a vertical dashed line and labeled r^*_{MS})

Also shown in Figure S6 are two least squares regression lines; a piecewise relationship consisting of these two fitted curves are utilized because there is a change in the relationship between MS signal and MFC ratio at higher analyte flow values. For the H_2 calibration curve in Figure S6, this transition occurs above a MS signal ratio of r^*_{MS} = 0.126. Figure S7 reports calibration data and fitted least squares regression relationships for other tracked analytes.

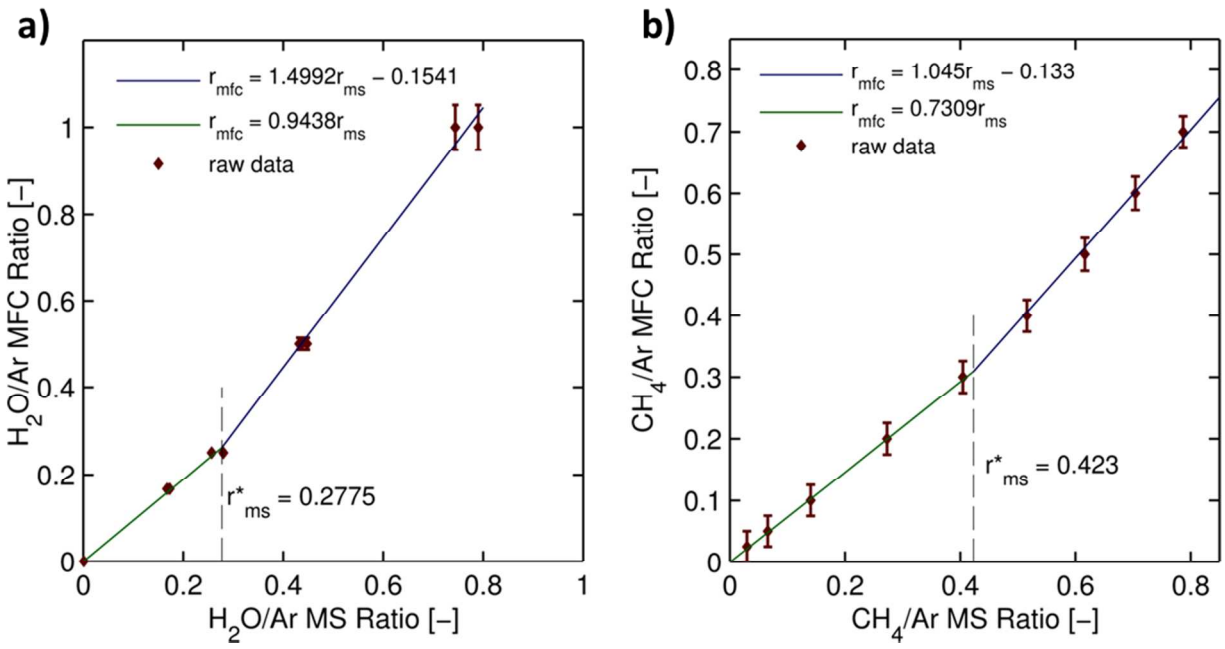

Figure S7: MS calibration and least squares fit lines for a) H_2O and b) CH_4

S3.2 Full CHAMP-SORB Experimental Procedure

The following procedure was carried out to demonstrate the reaction/adsorption/permeation step of the CHAMP-SORB reactor (refer to the P&ID in Figure S1 for valve labeling). During the entire experiment, a constant Ar flowrate of 200 sccm was metered through MFC 3, flowing across the backside of the Pd/Ag membrane and to the mass spectrometer.

(1) Valves E, G and H were opened and the reactor piston was moved to minimum volume as 15 sccm of helium flowed through the reactor to purge the system.

(2) Starting with the accumulator at the target operating pressure, the accumulator piston was moved downward to sweep a volume equal to that of the maximum volume of the CHAMP-SORB reactor (ensuring that after pressure equilibration between the CHAMP-SORB reactor and the fuel accumulator, the system should be at the target pressure).

(3) Valves E and H were closed and valve D was opened to send fuel to the CHAMP-SORB reactor.

(4) The reactor piston was moved to maximum volume and the inlet valve G was closed, isolating the system at a final pressure equal to the target operating pressure.

(5) As the reaction/adsorption/permeation process occurred, the piston compressed the reactor volume to maintain constant pressure using closed loop feedback, and the mass spectrometer measured hydrogen production rate; simultaneously, valve D was closed and valves E & F were opened to purge the feed line with He.
(6) Valve H was slowly opened to send remaining contents inside the reactor to the mass spectrometer.
(7) Valve G was opened to send 15 sccm of purge He to flush out remaining reactor contents.

S3.3 Experimental Uncertainty

The error bars in Figure S6 and Figure S7 are calculated using the uncertainty associated with the MFC measurements. In the case of H_2 and CH_4 calibration, the Ar flow was set at 200 sccm for the duration of the test. An MFC with a maximum flowrate of 5000 sccm was utilized, which has an accuracy of +/-1% of full scale, or +/-50 sccm. To substantially reduce experimental uncertainty, prior to conducting a calibration experiment the output of the MFC was sent to an Agilent ADM 1000 gas flow meter, and the MFC setting was adjusted until the target value of 200 sccm was detected by the ADM 1000. At this flowrate, the ADM 1000 has an accuracy of +/-6 sccm. To verify there was no drift during the test, at the conclusion of the calibration experiment the Ar MFC output was again sent to the ADM 1000 to ensure the same target 200 sccm reading was observed. In the H_2 and CH_4 calibration experiments, an MFC with a full scale of 500 sccm was used to control the analyte flow, giving an accuracy of +/-5 sccm.

For the H_2O calibration experiment, the sweep Ar flow was controlled with the 500 sccm full scale MFC, giving the same error as reported for the analyte in the H_2 or CH_4 calibration. The steam was introduced as liquid water, injected using a syringe pump (World Precision Instruments, SPI100i) with +/-0.05 ml/hr accuracy (equivalent to +/-1.19 sccm in vapor phase if recast using the density of an ideal gas at standard temperature and pressure). Using these uncertainty values, a standard error propagation analysis was employed to calculate the error in MFC flowrate ratio for species i to Ar:

$$e_{r_{MFC}} = \sqrt{\left[\left(\frac{\partial r_{MFC}}{\partial \dot{n}_i}\right) e_{\dot{n}_i}\right]^2 + \left[\left(\frac{\partial r_{MFC}}{\partial \dot{n}_{Ar}}\right) e_{\dot{n}_{Ar}}\right]^2} \quad \text{(S3)}$$

where the ratio of known flowrates metered by the mass flow controller $r_{MFC} = \dot{n}_i/\dot{n}_{Ar}$. Carrying out the partial differentiation of the equation describing r_{MFC}, eq S3 becomes:

$$e_{r_{MFC}} = \sqrt{\left[\left(\frac{1}{\dot{n}_{Ar}}\right) e_{\dot{n}_i}\right]^2 + \left[\left(-\frac{\dot{n}_i}{(\dot{n}_{Ar})^2}\right) e_{\dot{n}_{Ar}}\right]^2} \quad \text{(S4)}$$

The variation in error bars for the experimental range of MFC flowrate ratios for the H_2O calibration is greater than the variation seen in the H_2 or CH_4 calibration. This is due to the difference in calibration experimental procedure for a liquid as opposed to a gas analyte; the syringe pump flowrate was held constant during the H_2O calibration experiment, to avoid transient behavior in the evaporator as liquid flowrates varied. To achieve different MFC flow ratios in the liquid calibration experiment, the Ar sweep gas flowrate, as opposed to the analyte flowrate, was modulated (in this particular case in the range 100 – 500 sccm). This results in larger error bars at higher H_2O/Ar flowrate ratios in Figure S7a, as low values of Ar flow were required to achieve the desired flowrate ratio and the fixed +/-5 sccm error was a larger percentage of the target flowrate. The experimental error in MS signal ratio is determined using an identical approach to that of eq S3 and eq S4; however, the error bars are not displayed on Figure S6 and Figure S7 because they are within the width of the marker lines due to the high accuracy of the MS readings.

The error in effluent flow rates calculated from the full CHAMP-SORB experiments is also calculated with an error propagation analysis. The general relationship between the detected signal ratio and the true (in this case, unknown) ratio of analyte to sweep gas flowrates is given by the least squares regression lines fitted from the calibration data (expressed in the general form $r_{MFC} = m_i r_{MS} + b$, where m_i and b are the slope and y-intercept, respectively, of the fitted data). It then follows that the flowrate of the unknown analyte relative to the known sweep gas flowrate is:

$$\dot{n}_i = \dot{n}_{Ar}(m_i r_{MS} + b) \tag{S5}$$

Eq S5 is used in conjunction with the error propagation analysis to determine the experimental error of any effluent from the reactor as it is detected by the mass spectrometer:

$$e_{\dot{n}_i} = \sqrt{\left[\left(\frac{\partial \dot{n}_i}{\partial \dot{n}_{Ar}}\right) e_{\dot{n}_{Ar}}\right]^2 + \left[\left(\frac{\partial \dot{n}_i}{\partial r_{MS}}\right) e_{r_{MS}}\right]^2} \tag{S6}$$

The results of the error bar estimation for the representative full CHAMP-SORB test are reported in Figure S8. For clarity, even though data were collected during the experiment at a frequency of approximately 0.7 seconds, only data points per 25 seconds are shown to reduce clutter of visual representation.

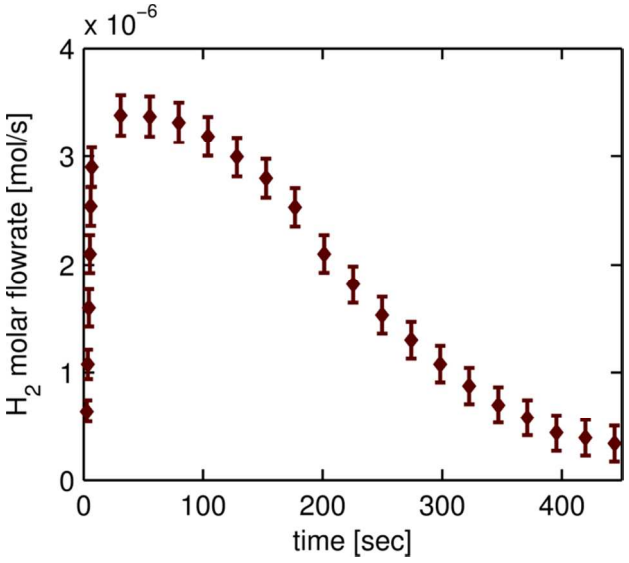

Figure S8: Representative flowrates with error bars for representative CHAMP-SORB run (presented in Figure 3a of the main paper)

S4. Characterization and System Conditioning

Prior to each CHAMP-SORB reactor run, background experiments were conducted to characterize each of the CHAMP-SORB reactor sub-functions (*i.e.* reactor filling, permeation, adsorption and reaction). Each of these activities is described in detail in the following sections.

S4.1 Reactor Filling

Obtaining a batch of fuel mixture at the target total pressure with the appropriate S/C ratio (for this experiment a 2:1 ratio) is somewhat challenging due to the difference in phase at room temperature between H_2O (liquid) and CH_4 (gas). To accomplish this task, the accumulator was first heated to 200°C and filled with CH_4 at 1/3 of the target pressure. The filling process was comprised of first flowing CH_4 through the accumulator and out the downstream vent with the accumulator piston at minimum displacement (to flush out all non-CH_4 species), then closing the outlet valve and moving the accumulator piston to maximum displacement while opening connection of the accumulator to the pure CH_4 supply line. At this point, the heat tracing on the inlet line ("zone 1" in Figure S1) was turned off such that the temperature in the inlet line to the accumulator was approximately 25°C. Simultaneously, the heat tracing in "zone 2" was turned on to heat that portion of the line and outlet valve to 200°C.

After filling the accumulator with CH_4 at 1/3 the final target pressure, valve A was closed, valve B was opened, and the three way valve C was switched to a position such that any liquid water pumped was directed to the vent rather than the accumulator. This process ensured that the line was fully primed with water and that when valve C was subsequently switched to direct flow towards the accumulator, any additional quantity of water pumped by the syringe pump would cause an equal amount of water to enter the accumulator rather than to fill the piping connecting valves B and C. An amount of liquid H_2O corresponding to twice the number of moles of CH_4 in the accumulator (as determined using the ideal gas equation of state) was then injected into the accumulator with the syringe pump. For a target final pressure of 5 bar with CH_4 in the accumulator initially at 1/3 this pressure, this required an injection of 30 mL of liquid water at room temperature. Finally, valve C is closed and power is supplied to the zone 1 heater to vaporize the water. Figure S9 illustrates the rise in temperature and pressure (due to water vaporization) as zone 1 is heated to 200°C.

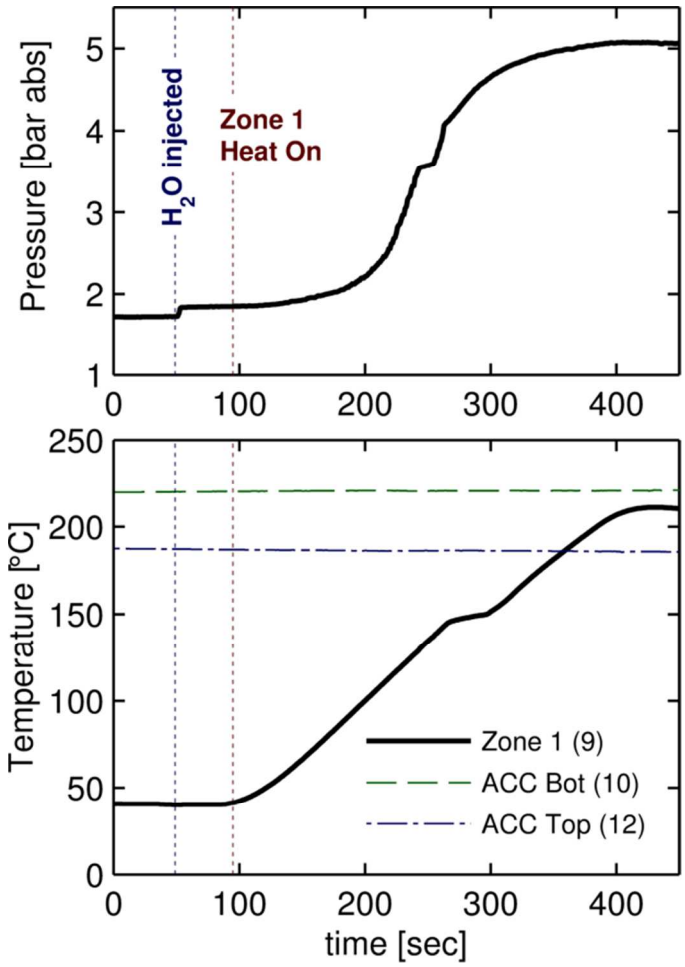

Figure S9: Transient response of a) the accumulator pressure, and b) the temperature measurements at "zone 1" and in the top and bottom of the accumulator during the vaporization of the injected liquid water.

The fact that the final pressure in the accumulator did in fact reach 5 bar, a value three times greater than the initial fill pressure of pure CH_4, provides confidence that the S/C ratio in the accumulator after following this filling process is the desired 2:1 value. To further verify an accuracy of this approach of forming a mixture with a desired S/C ratio, a fraction of the mixture contained in the accumulator was sent to the CHAMP-SORB reactor for a brief (*ca.* 20 seconds) duration and then transmitted to mass spectrometer using the same flushing process outlined in steps (6)-(7) of the full test procedure. The CHAMP-SORB reactor was not fitted with any catalyst or sorbent during this experiment, so that the water-methane mixture would remain as supplied (*i.e.*, no change in species due

to reaction or adsorption) and the S/C ratio could be tested using the mass spectrometer measurements. The results are presented in Figure S10.

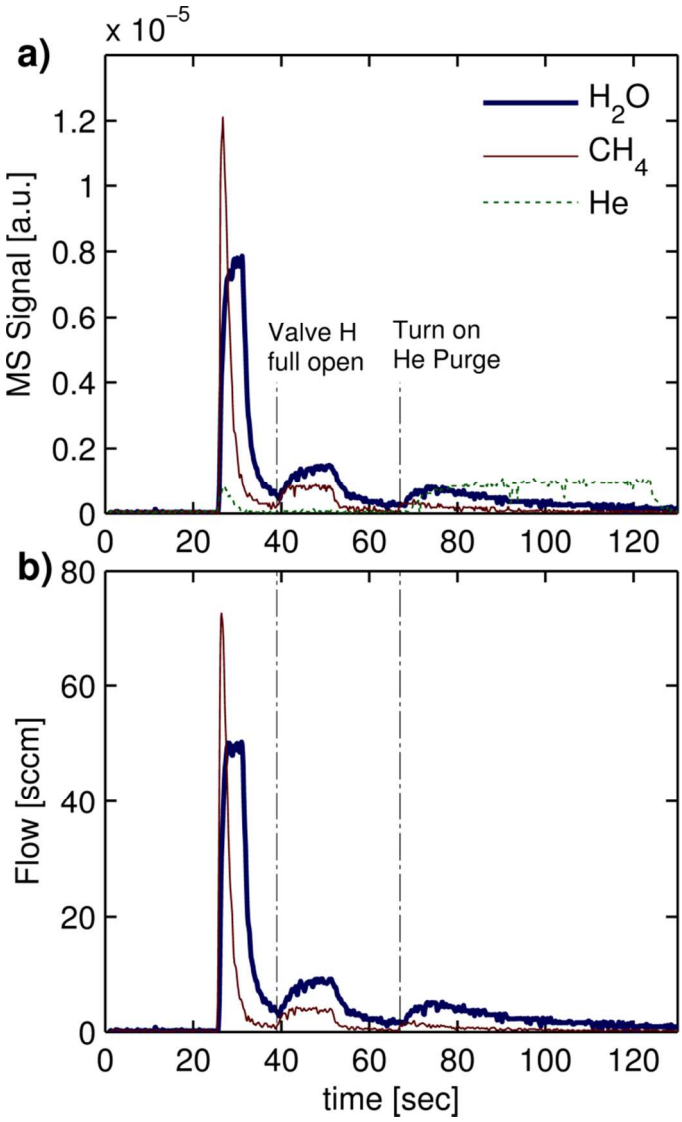

Figure S10: a) Measured MS signals and b) calculated H_2O and CH_4 flowrates from experiments designed to independetnly verify achievement of target S/C ratio in the accumulator

There is large spike in MS signal of H_2O and CH_4 when the outlet valve (H) is initially cracked due to the difference in pressure between the reactor (initially at 5 bar) and the sweep gas line (at atmospheric pressure). This initial spike followed by two secondary peaks: first, when the outlet valve was fully opened, and secondly when He was swept through the reactor to purge out any contents that remain

after pressure equilibration. The calculated CH_4 and H_2O flow rates reported in Figure S10 are then integrated in the time domain to determine total number of moles of each species present in the reactor. The potential range of values in the calculation of total moles of CH_4 or H_2O is determined by integration using the high and low bound values, as determined in the previously outlined error propagation analysis. The summary of 3 separate filling tests, using a single batch of fuel generated in the accumulator (the same batch used in obtaining data shown in Figure S9) is reported in Table S1. The maximum bounding values of S/C ratio for each experiment are calculated using the maximum moles of H_2O divided by the minimum moles of CH_4 as determined by integrating the molar flowrates. Similarly, minimum bounding values of S/C ratio are determined using the ratio of the minimum number of moles for H_2O to the maximum number of moles for CH_4, and these values are used to determine the reported uncertainty in Table S1.

Table S1: Calculated S/C ratio from fill test

Experiment	S/C Ratio	
	Nominal Value	Uncertainty
1	2.06 : 1	+/- 0.17
2	2.27 : 1	+/- 0.19
3	2.17 : 1	+/- 0.21
MEAN	**2.17 : 1**	**+/- 0.19**

The calculations in Table S1 show some spread in data between three separate reactor filling experiments from the same water-methane mixture batch prepared in the accumulator, with the mean S/C ratio being slightly above the target 2:1 value (2.17:1). However, the target (2:1) S/C ratio falls within the bounds of uncertainty around the experimentally observed mean value, and it is expected that the ratio of partial pressures (as determined using the pressure of pure methane in the accumulator prior to adding liquid water and heating above saturation temperature, along with the final pressure

after heating) is a more accurate representation of the true S/C ratio because there is less error in the direct pressure transducer measurement than the error propagation of the indirect mass spectrometer measurement.

S4.2 Membrane Conditioning and Permeance Validation

The H_2-selective membrane (Alfa Aesar, 50 μm thick, 77% Pd/23% Ag) was conditioned by being wrapped in aluminum foil and heated to 650°C in a furnace for 3 hours prior to installation in the CHAMP-SORB reactor. After conditioning, the membrane was fitted in the CHAMP-SORB reactor, and the reactor was filled with inert He as quickly as possible to minimize exposure to potential contaminants and metal oxidants in the air. The reactor was then heated to the typical operating condition of 400°C filled with inert He at atmospheric pressure. The reactor inlet valve was subsequently opened and exposed to the H_2 tank regulated at 5 bar total pressure, such that an initial gas mixture of four parts H_2 to one part He was achieved in the reactor upon equilibration. Argon sweep gas at a 200 sccm flowrate was sent through the backside of the membrane to maintain a low permeate-side H_2 partial pressure and carry the permeated hydrogen to the mass spectrometer for detection. Once the inlet valve was closed, the volume was held constant so that no more H_2 could enter the reactor, and as a result the reactor pressure decayed exponentially to a value approaching atmospheric pressure. Figure S11 reports the resulting rate of pressure decay observed in 5 separate experiments.

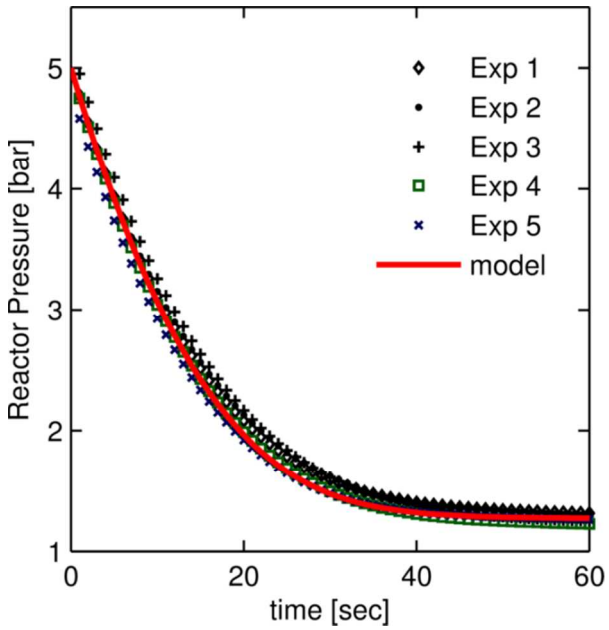

Figure S11: Reactor pressure decay as a result of H_2 permeation for 5 separate experiments. Solid line shows the modeled pressure decay rate using Sievert's law for hydrogen permeation using membrane permeance from McLeod et al.[1]

Also shown in Figure S11 is the predicted pressure decay using Sievert's Law and a membrane permeance of $D_{mem} = 4.1 \times 10^{-5}\, exp\{-1387.9/T\}\ [mol \cdot m/(m^2 \cdot s \cdot bar^{1/2})]$ measured by McLeod et al.[1] The prediction is modeled through the use of eqs S7 and S8, where S7 relates the rate of pressure drop in the reactor (dP/dt, which is equal to the time rate of change in H_2 partial pressure dP_{H_2}/dt because the number of moles of inert He remains constant) to the time rate of change in moles of H_2 (dN_{H_2}/dt) and is derived by taking the time derivative of the ideal gas equation of state with temperature T and volume V being held constant.

$$\frac{dP_{H_2}}{dt} = \left(\frac{R_u T}{V}\right)\frac{dN_{H_2}}{dt} \tag{S7}$$

The time rate of change in number of moles of H_2 in the reactor is modeled using Sievert's Law:

$$\frac{dN_{H_2}}{dt} = -A_c \frac{D_{mem}}{\delta}\left[\left(P_{H_2}\right)^{1/2} - \left(P_{H_2}^{\infty}\right)^{1/2}\right] \tag{S8}$$

The ordinary differential equation resulting from insertion of the expression for dN_{H_2}/dt back into eq S7 is then solved numerically as an initial value problem (with initial condition of $P_{H_2}\big|_{t=0} = 4$ bar to

match the experimental test conditions). This solution is carried out in MATLAB using the built-in ode45 solver, an explicit Runge-Kutta Dorman-Prince (RKDP) scheme accurate to the order of $O(\Delta t^4)$.[2] A permeate-side H_2 partial pressure value of $P_{H_2}^{\infty}$ = 0.1 bar is chosen in the simulations to match the experimentally observed final total pressure in the reactor of approximately 1.1 bar (due to inert He at atmospheric pressure and residual, unpermeated H_2 at 0.1 bar). The excellent match in pressure decay rate due to H_2 permeation between the experiments and simulations, with no adjustment or use of empirical factors, displayed in Figure S11 validates the applicability of Sievert's law to describe H_2 permeation in the CHAMP-SORB reactor and the use of McLeod et al.'s value for Pd/Ag membrane permeance.

S4.3 CO_2 Adsorbent Preparation and Performance Validation

The CO_2-selective sorbent was prepared by impregnating a base material of Pural MG 70 hydrotalcite (Sasol) with K_2CO_3 (Sigma Aldrich). The resulting sorbent was 78% by weight hydrotalcite, 22% by weight K_2CO_3. A batch of 25g of sorbent was produced as follows using the incipient wetness procedure:[3]

(1) 19.5 g of Pural MG 70 was distributed evenly in a porcelain bowl.
(2) An aqueous solution of K_2CO_3 was prepared by dissolving 5.5 g of K_2CO_3 in 10 mL of deionized water.
(3) Half of the aqueous K_2CO_3 solution was added to the MG 70 powder, and the wet powder was mixed and spread again evenly in the bowl.
(4) The remainder of the aqueous K_2CO_3 solution was added to the powder and mixed.
(5) The wet powder was dried for 12 hours in a fume hood at room temperature.
(6) After 12 hours, the powder was placed in an oven at 120°C for 6 hours to complete drying.
(7) The temperature of the dried mixture was elevated from 120 to 400°C at a 3°C/min ramp rate, and then held at 400°C for 3 hours for calcination.
(8) The calcined sorbent was crushed and sieved to a diameter range of 0.124-0.297 mm.

To validate that the K_2CO_3-promoted hydrotalcite sorbent would adsorb CO_2 as intended, two experiments were conducted. The first of these was a test similar to the pressure decay experiment described in Section S4.3, where a gas mixture at roughly 5 bar total pressure, comprised of an inert gas (in this case Ar) at atmospheric partial pressure with balance CO_2 (as opposed to H_2 in the permeation testing) is introduced into the testbed CHAMP-SORB reactor. For this experiment, the reactor is loaded with 0.25 g of sorbent and heated to 400°C. The reactor is held at a constant volume and the pressure decay is recorded and used to estimate the rate of CO_2 adsorption (using the ideal gas equation of state). There was a small leak of 0.07 bar/min estimated when the reactor was filled with pure (inert) Ar at 5 bar, and measured to be the same rate both before and after the batch adsorption test. As a result, the pressure decay data presented in Figure S12 was adjusted for this constant decay rate, assuming that the same leak rate holds when reactor is filled with CO_2/Ar mixture to the same initial pressure. The batch CO_2 uptake experiment was conducted twice to ensure repeatability, and prior to each test the sorbent bed was purged with inert Ar gas for 15 minutes (at which point no CO_2 was detected in the effluent to the mass spectrometer) to ensure that the sorbent was initially not loaded with any CO_2.

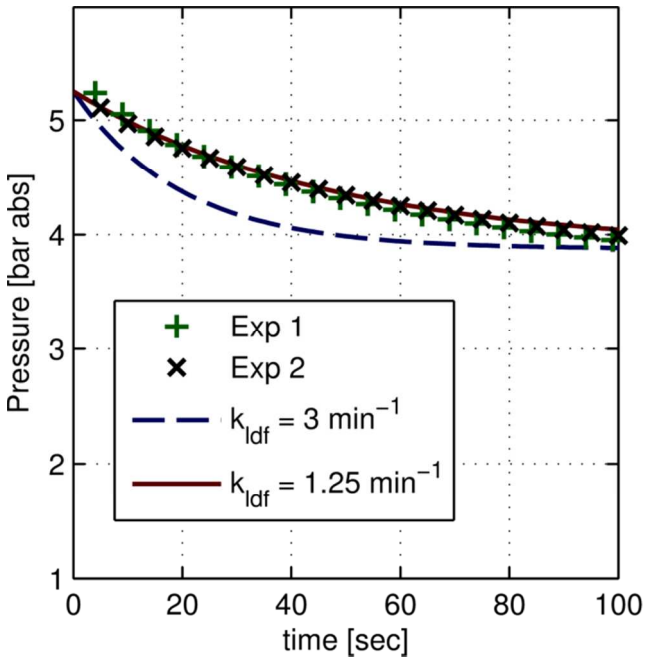

Figure S12: Reactor pressure decay during sorption CO_2 uptake – experiments and model predictions using various values of adsorption coefficient in linear driving force model

Also shown in Figure S12 are two predicted pressure decay curves for different linear driving force adsorption coefficients (k_{ldf}). Similar to the differential equation used to describe the change in reactor pressure (at constant volume and temperature) during the permeation experiment, according to the ideal gas equation of state the change in pressure during the batch CO_2 uptake experiment is expected to be of the following form:

$$\frac{dP_{CO_2}}{dt} = -\left(\frac{R_u T}{V}\right)\left[m_{sorb}\frac{dq_{CO_2}}{dt}\right] \quad \text{(S9)}$$

For the batch CO_2 uptake experiment, the time rate of change in moles of CO_2 in the reactor (the last term in brackets in eq S9) is the product of the mass of the sorbent (m_{sorb}) and the time rate of change of CO_2 loaded on the sorbent per unit mass (dq_{CO_2}/dt). The specific rate of CO_2 adsorption can be modeled using the linear driving force approach:

$$\frac{dq_{CO_2}}{dt} = k_{ldf}\left[q_{eq} - q_{CO_2}\right] \quad \text{(S10)}$$

where q_{CO_2} is the current loading of CO_2 per unit mass of sorbent and q_{eq} is the equilibrium loading of CO_2 at the current temperature and CO_2 partial pressure. At a temperature of 400°C, the linear driving force coefficient for the K_2CO_3-promoted hydrotalcite sorbent reported by Lee et al. is 3 min^{-1}.[4] The relationship between equilibrium CO_2 loading and CO_2 partial pressure is also taken from Lee et al., and the initial value problem with these coupled ordinary differential equations (with an initial pressure $P_{CO_2}\big|_{t=0}$ = 4.25 bar and initial sorbent loading $q_{CO_2}\big|_{t=0}$ = 0 mol/kg, to match experimental conditions) is again solved numerically in MATLAB using the ode45 RKDP numerical integration routine. The results of this numerical solution, for two possible k_{ldf} values, are shown in Figure S12. The reported value in the literature of 3 min^{-1} overestimates the adsorption rate, but adjusting the linear driving force coefficient to 1.25 min^{-1} provides a match to the experimental data.

Because the measurements of pressure in the batch CO_2 uptake experiment only indirectly measure the CO_2 adsorption rate and are somewhat confounded by the slight leak in the system, a packed bed CO_2 adsorption experiment was also conducted to verify through direct measurement that the sorbent was in fact effective in capturing CO_2. The packed-bed experimental apparatus built for this experiment is illustrated in Figure S13.

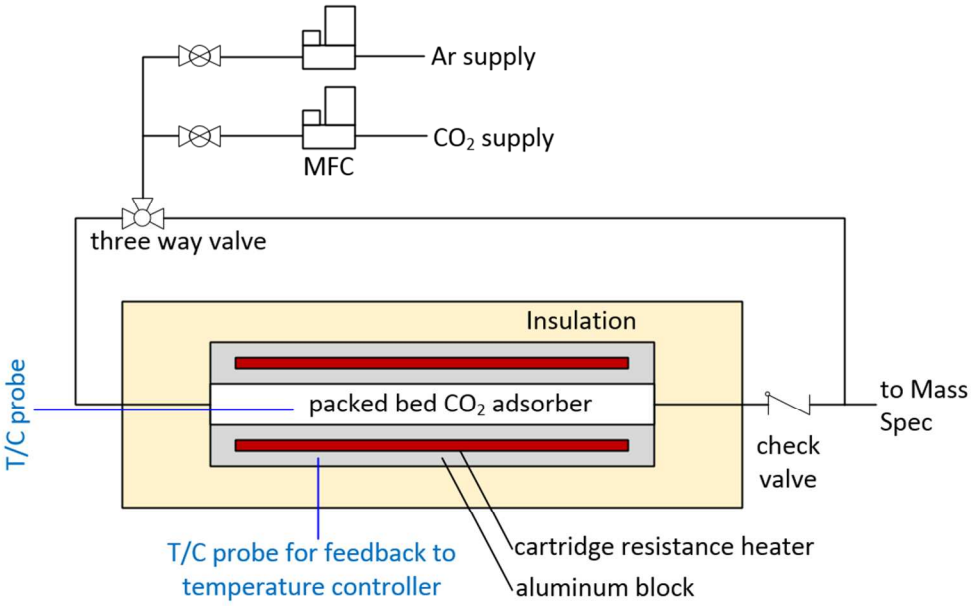

Figure S13: Experimental apparatus for packed bed CO_2 uptake experiment

The system consisted of ¼-inch stainless steel tube segment, surrounded by heated aluminum blocks and encased in rigid calcium silicate insulation. The tubular reactor was packed with sorbent and heated to 400°C using the Harrick 24V automatic temperature controller. Using mass flow controllers, a metered mixture of CO_2 (8 sccm) in inert Ar sweep gas (30 sccm) was first sent directly to the mass spectrometer, bypassing the reactor, to detect the pure CO_2 MS signal. Once this baseline signal was established, the three way valve was switched such that the CO_2/Ar mixture was diverted to flow through the packed bed adsorber prior to reaching the mass spectrometer. The results of the packed bed CO_2 uptake experiment are shown in Figure S14.

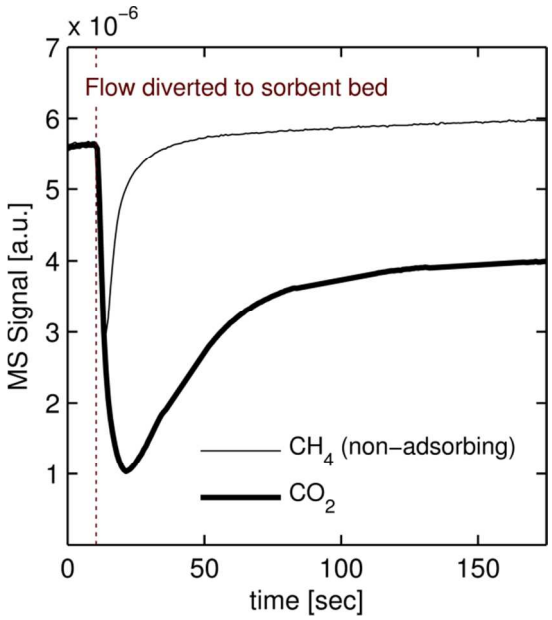

Figure S14: Reduction of MS signal of analyte (adsorbing CO_2 or non-adsorbing CH_4) due to flow diversion from bypass to through packed bed adsorber to confirm CO_2 adsorption

As can be seen by the drop in MS Signal for CO_2 once flow is diverted to the sorbent bed, there was a reduction in the relative amount of CO_2 that reached the mass spectrometer. Because the adsorber column is initially filled with inert Ar, the drop in CO_2 signal is partially due to the time required for the flowing CO_2-Ar mixture to displace that pure Ar. To identify how much of the detected reduction in CO_2 signal at the MS was due to the displacement effect, the same test procedure was carried out with a non-adsorbing species (CH_4) at the same 8 sccm/30 sccm analyte to carrier gas flow ratio. Figure S14 illustrates that, although there was a drop in CH_4 MS signal at the moment of flow diversion to the adsorber bed, this drop was much shorter in duration than the time period during which the CO_2 signal drop is observed. Additionally, the CH_4 signal recovered fully to its pre-diverted value, while the CO_2 signal remained at approximately 2/3 of its initial value. The fact that the CO_2 signal did not fully vanish (i.e., indicative of complete CO_2 adsorption) after flowing through the packed bed column is likely because there was insufficient residence time in the reactor for complete adsorption; this is supported by the fact that the residence time (estimated to be *ca.* 25 seconds, as indicated by the duration of the

drop in the MS signal of non-adsorbing CH_4 in Figure S14) is approximately half the intrinsic adsorption timescale ($\tau_{ads,intrinsic} \sim 1/k_{ldf}$, or 48 seconds using the estimated k_{ldf} of 1.25 min^{-1} from the batch adsorption experiment). Regardless of the incomplete adsorption, the experiment was successful in that its purpose was to obtain a direct, but strictly qualitative, confirmation that CO_2 was indeed being adsorbed (as opposed to the indirect pressure decay measurements obtained in the batch CO_2 uptake experiments).

S4.4 Catalyst Reduction and Activity Verification

The nickel on calcium aluminate catalyst (Alfa Aesar, HiFuel R110) is supplied in oxidized form, and prior to use in the CHAMP-SORB reactor must be reduced to convert the surface NiO to Ni. The supplier instructions state that the catalyst should be exposed to dry hydrogen at 600°C for a minimum of two hours. Because the CHAMP-SORB reactor, as designed for laboratory experiments, cannot reach a temperature this high (in order to maintain integrity of the seal material), the reduction procedure was carried out in the packed bed reactor as introduced in Figure S13. In this case, pure H_2 metered by a mass flow controller was flowed through reactor filled this time with crushed catalyst as opposed to sorbent. Two means of verifying the reduction process were employed: 1) the catalyst temperature was monitored using a K-type thermocouple to look for a temperature rise due to initiation of the exothermic reduction process, and 2) the effluent of the packed bed was monitored for H_2O content (as H_2O will be the product of the reduction of NiO to Ni in the presence of dry H_2).

Figure S15 reports the time evolution of temperature and MS signal measurements obtained during the catalyst reduction procedure. When the H_2 flow was turned on, approximately 30 seconds into data collection, both H_2 and H_2O were detected by the mass spectrometer. Simultaneously, the catalyst temperature rose from 600 to 608°C and the required output from the Harrick temperature controller to maintain the aluminum heater block at a constant value of 600°C was reduced by several percent (due to the heat generation from the exothermic catalyst reduction reaction).

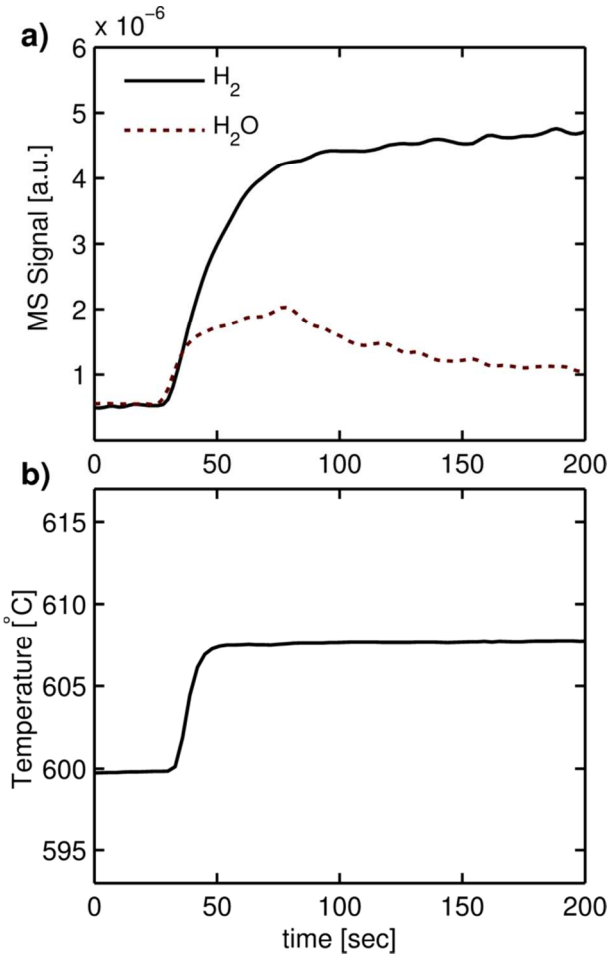

Figure S15: Measurements of a) effluent mass spectrometer signal and b) catalyst temperature during the catalyst reduction procedure. The presence of H_2O in the effluent and the rise in temperature (due to exothermic metal oxide reduction reaction) verify occurrence of the catalyst reduction process.

Although not shown in Figure S15, the catalyst reduction was carried out for four hours, twice the minimum value specified by the supplier. Periodically during the reduction, the H_2 flow was shut off and each time the temperature measured in the catalyst gradually dropped to 600°C, then rose back to near 610°C when the H_2 flow was resumed. Once the reduction was complete, the second experiment was conducted to verify catalyst activity by first flushing the reactor with Ar, then replacing the H_2 feed with CH_4 and steam in a 2:1 S/C mass flow ratio, with water supplied through a syringe pump and evaporator to the packed bed reactor inlet. The results of this experiment, illustrated in Figure S16, confirm that all the expected products of the SMR process (H_2, CO_2 and CO) are present in the effluent of the reactor.

Similar to the packed bed adsorption experiment, the purpose of this test was to qualitatively confirm the occurrence of SMR (as opposed to a detailed study of the kinetics).

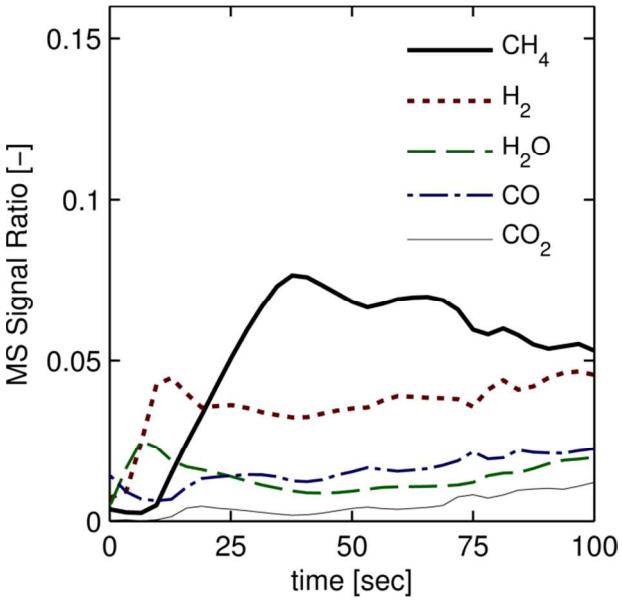

Figure S16: Packed bed reactor effluent with a 2:1 S/C ratio H_2O:CH_4 feed after catalyst reduction, confirming the presence of the expected products of the SMR process (H_2, CO_2, CO)

S5. Supplementary Experimental Results

In addition to the results from a fully operational CHAMP-SORB reactor in Figure 3 of the main paper, which reports the permeate-side H_2 mass spectrometer signal as well as pressure and piston height during a representative experiment, Figure S17 reports the H_2 MS signal for three separate constant pressure CHAMP-SORB experiments. The same qualitative behavior is evident in all three experiments; the H_2 permeation rate remains elevated initially while the reactor can sustain constant pressure, until it tapers off when no more working volume is available in the system (at approximately $t = 150\ sec$). Also shown in Figure S17 is a constant volume experiment for comparison, where the piston of the CHAMP-SORB reactor is fixed for the duration of the fuel batch residence time.

Without compression provided during the beginning of the process, the permeation rate begins to decay immediately as pressure drops in the reactor and a clear reduction in reactor performance is evident.

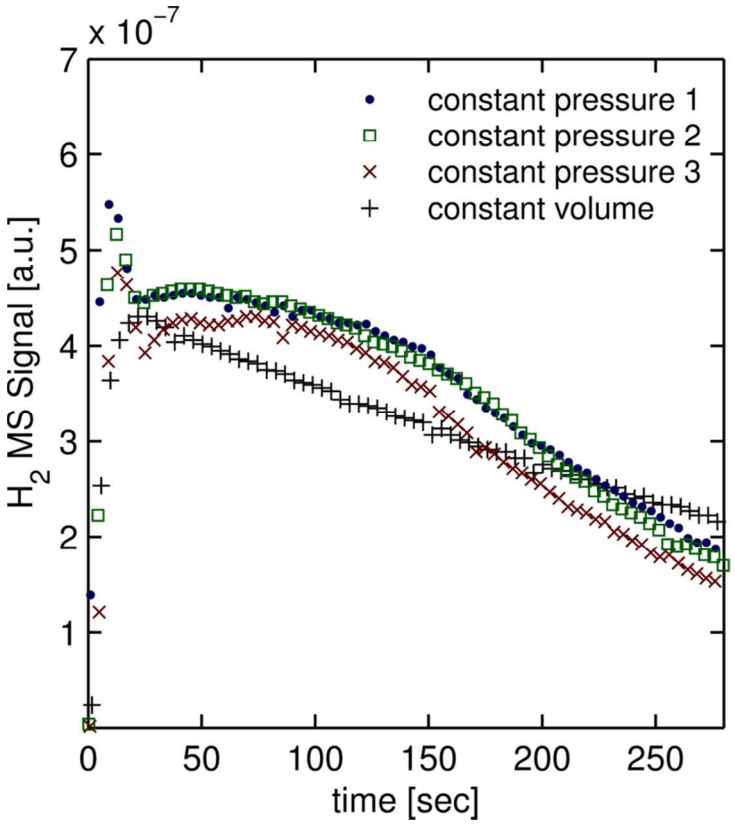

Figure S17: CHAMP-SORB experimental results showing reactor effluent H_2 MS signal for multiple constant pressure experiments, contrasted with the H_2 MS signal for a constant volume operation mode.

Additionally of interest is the temperature at the catalyst during the full CHAMP-SORB experiment; a plot of temperature versus time corresponding to the experiments reported in Figure 3 of the primary manuscript is shown in Figure S18. Initially the temperature drops by roughly 2-3°C due to the endothermic reaction. At around 200 seconds the temperature drops again by about 2°C as the piston reaches the top of the catalyst (which occurs at the same time), when the piston is at a slightly lower temperature and as such some additional heat losses are observed via conduction from the catalyst to the piston. The subsequent rise in temperature is due to correction from the PID controller making up for heat lost to the piston. Regardless, the total temperature change from the target operating

temperature of 400°C is approximately 4°C (owing to the small nature of the testbed reactor and use of the PID controller targeting a fixed operating temperature), justifying the use of an isothermal analysis in the corresponding kinetic model.

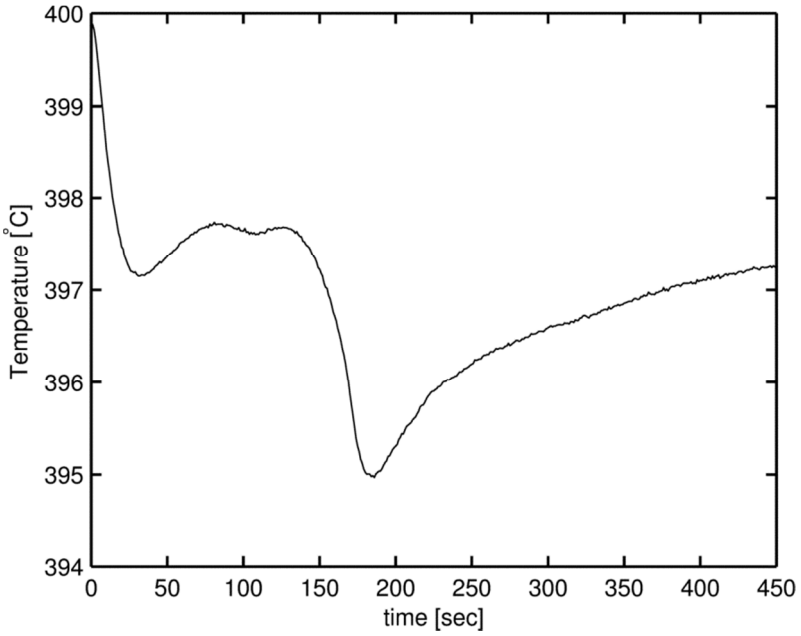

Figure S18: Catalyst temperature during the CHAMP-SORB reaction step shown in Figure 3 of the main manuscript

S6. Kinetic Model Parameters

S6.1 Sorbent Equilibrium Isotherm and Kinetic Data

The equilibrium and kinetic data of Lee et al. [4] is used for the adsorption model, as opposed to other studies on K_2CO_3-promoted hydrotalcite reported in the literature, because that study is the only one that measured the CO_2 adsorption isotherm up to the high CO_2 partial pressure range expected to be encountered during CHAMP-SORB operation.[5] According to the model proposed by Lee et al. [4], CO_2 can be adsorbed to the surface of K_2CO_3-promoted hydrotalcite in two ways: (1) chemisorbed directly on a surface (S) site forming ($CO_2 - S$), or (2) as a surface complex (where a molecules of CO_2 in gas phase react with the chemisorbed CO_2 molecule to form a surface complex of the form $(CO_2)_{a+1}$):

$$CO_2(gas) + S \rightleftharpoons CO_2 - S \quad \text{(S11)}$$

$$aCO_2(gas) + CO_2 - S \rightleftharpoons (CO_2)_{a+1} - S \quad \text{(S12)}$$

This adsorption model results in an equilibrium isotherm describing the CO_2 adsorption capacity (q_{eq}) as a function of temperature (T) and CO_2 partial pressure (P_{CO_2}) of the form:

$$q_{eq}(P_{CO_2}, T) = \frac{mK_C P_{CO_2}\left[1 + (a+1)K_R P_{CO_2}^{a}\right]}{\left[1 + K_C P_{CO_2} + K_C K_R P_{CO_2}^{(a+1)}\right]} \quad \text{(S13)}$$

where K_C (units $[bar^{-1}]$) and K_R (units $[bar^{-a}]$) are the equilibrium constants of the chemisorption (eq S11) and chemical complexation (eq S12) reactions, respectively, and m (units $[mol/kg]$) is the capacity of moles per unit mass available for chemisorbed CO_2 on the sorbent material. As such the maximum possible loading of CO_2 on the sorbent (in the limit of $P_{CO_2} \to \infty$) is $m(a+1)$ mol/kg. The rate at which the sorbent's specific CO_2 loading (q_{CO_2}) approaches the equilibrium value (given by eq S13) is estimated using a linear driving force approach,[6] where the rate of adsorption is directly proportional to the difference between equilibrium and instantaneous CO_2 loading at that point in time, as indicated by eq S10 in Section S4.3. The parameters K_C, K_R, a and k_{ldf} have an exponential dependence on the inverse of temperature of the form $y = y^0 exp\{\Delta E_y / R_u T\}$. Value of the pre-exponential factor (y^0) and activation parameter (ΔE_y) for K_C and K_R are given explicitly by Lee et al. The value of these parameters for a and k_{LDF} are estimated by fitting a line for $\ln\{a\}$ or $\ln\{k_{ldf}\}$ versus $1/T$ between data points given at two temperatures ($a = 2.5$, $k_{ldf} = 3\ min^{-1}$ at $T = 673K$, and $a = 1.8$, $k_{ldf} = 5\ min^{-1}$ at $T = 793K$). Determination of these parameters, listed in Table S2, allows for implementation of the adsorption model at temperatures other than the two values explicitly listed in Lee et al.[4, 7]

Table S2: Pre-Exponential Factor and Activation Parameter for K_2CO_3-Promoted Hydrotalcite Adsorption Model[4, 7]

Parameter	Parameter Expression	Pre-Exponential Factor	Activation Parameter
$K_C\ [bar^{-1}]$	$K_C = K_C^0 exp\{q_C/R_u T\}$	$K_C^0 = 0.8665\ [bar^{-1}]$	$q_C = 21.0\ [kJ/mol]$
$K_R\ [bar^{-a}]$	$K_R = K_R^0 exp\{\Delta H_R/R_u T\}$	$K_R^0 = 1.30 \times 10^{-3} [bar^{-a}]$	$\Delta H_R = 42.2\ [kJ/mol]$
$a\ [-]$	$a = a^0 exp\{\Delta E_a/R_u T\}$	$a^0 = 0.2821$	$\Delta E_a = 12.21\ [kJ/mol]$
$k_{ldf}\ [min^{-1}]$	$k_{ldf} = k_{ldf}^0 exp\{\Delta E_k/R_u T\}$	$k_{ldf}^0 = 87.4\ [min^{-1}]$	$\Delta E_k = -18.85\ [kJ/mol]$

S6.2 Ni-based SMR Catalyst Intrinsic Reaction Rates

The kinetic model proposed by Xu and Froment[8] is used to model the chemical reaction rates of the reverse methanation, water gas shift, and overall steam methane reforming reactions. The rate of reaction i is a function of the partial pressure of each species j in the reactor (P_j), the equilibrium constants for that reaction (K_i where $i = RM, WGS\ or\ SMR$), and of the adsorption equilibrium constant of each species j onto the catalyst surface (K_j where $j = CO, H_2, CH_4\ or\ H_2O$). The rate expressions for the three reactions are given in Table S3.

Table S3: Kinetic Rate Expressions for SMR Process[8]

Reaction	Rate Expression $[mol/kg \cdot hr]$	Equilibrium Constant
$CH_4 + H_2O \rightleftharpoons 3H_2 + CO$	$r_{RM} = \frac{k_{RM}/P_{H_2}^{2.5}\left(P_{CH_4}P_{H_2O} - P_{H_2}^3 P_{CO}/K_{RM}\right)}{1 + K_{CO}P_{CO} + K_{H_2}P_{H_2} + K_{CH_4}P_{CH_4} + K_{H_2O}P_{H_2O}/P_{H_2}}$	$K_{RM} = exp\left\{30.11 - \frac{26{,}830}{T}\right\} \times 10^{-2}\ [bar^2]$
$CO + H_2O \rightleftharpoons H_2 + CO_2$	$r_{WGS} = \frac{k_{WGS}/P_{H_2}\left(P_{CO}P_{H_2O} - P_{H_2}P_{CO_2}/K_{WGS}\right)}{1 + K_{CO}P_{CO} + K_{H_2}P_{H_2} + K_{CH_4}P_{CH_4} + K_{H_2O}P_{H_2O}/P_{H_2}}$	$K_{WGS} = exp\left\{-4.036 - \frac{4{,}400}{T}\right\}\ [-]$
$CH_4 + 2H_2O \rightleftharpoons 4H_2 + CO_2$	$r_{SMR} = \frac{k_{SMR}/P_{H_2}^{3.5}\left(P_{CH_4}P_{H_2O}^2 - P_{H_2}^4 P_{CO_2}/K_{SMR}\right)}{1 + K_{CO}P_{CO} + K_{H_2}P_{H_2} + K_{CH_4}P_{CH_4} + K_{H_2O}P_{H_2O}/P_{H_2}}$	$K_{SMR} = K_{RM}K_{WGS}$

The adsorption equilibrium constant for species j (K_j) is of the form $K_j = K_j^0 exp\{\Delta H_j/R_u T\}$, where K_j^0 is the pre-exponential factor and ΔH_j is the heat of chemisorption of species j onto the catalyst surface. The rate constant for reaction i (k_i) follows the form of the Arrhenius expression $k_i = k_i^0 exp\{E_{a,i}/R_u T\}$, where k_i^0 is the pre-exponential factor and $E_{a,i}$ is the activation energy of reaction i. The values of these parameters are given by Xu and Froment and are listed in Table S4.

Table S4: Kinetic Parameters for SMR Process[8]

Parameter	Pre-Exponential Term k_i^0 or K_j^0	Activation Energy ($E_{a,i}$) or Heat of Chemisorption (ΔH_j)
k_{RM}	4.225×10^{18} $[mol \cdot bar^{1/2}/kg_{cat} \cdot hr]$	240.1 $[kJ/mol]$
k_{WGS}	1.955×10^{9} $[mol/kg_{cat} \cdot hr \cdot bar]$	67.13 $[kJ/mol]$
k_{SMR}	1.020×10^{18} $[mol \cdot bar^{1/2}/kg_{cat} \cdot hr]$	243.9 $[kJ/mol]$
K_{CO}	8.23×10^{-5} $[bar^{-1}]$	-70.65 $[kJ/mol]$
K_{H_2}	6.12×10^{-9} $[bar^{-1}]$	-80.29 $[kJ/mol]$
K_{CH_4}	6.65×10^{-4} $[bar^{-1}]$	38.28 $[kJ/mol]$
K_{H_2O}	1.77×10^{-5} $[-]$	88.68 $[kJ/mol]$

In the ideal kinetic model, when the rate expressions are implemented the rate of production of species j is given as follows:

$$r_{prod,j} = m_{cat} \sum_{i=1}^{3} \nu_{ij} r_i \quad \text{(S14)}$$

Where m_{cat} is the mass of catalyst (m_{cat}), ν_{ij} is the stoichiometric coefficient of reaction i, and r_i is the rate of each individual as determined using Table S3 and Table S4. To avoid singularities in the rate expression, any time the partial pressure of H_2 in the reactor is below a minimum value of $P_{H_2,min} = 0.001\ bar$ during a reactor simulation, that minimum value is utilized (as opposed to $P_{H_2} = 0\ bar$) in calculating the rates r_{RM}, r_{WGS} and r_{SMR}. This is only necessary during the initial several milliseconds of the reactor simulation, where the reactor initially contains pure fuel (and no H_2).

In addition to using catalyst particles of a sufficiently small size such that pellet internal mass transfer were not observed in Xu and Froment's kinetics study, the assumption of negligible intra particle diffusion resistance is further justified by calculation of the Weisz-Prater criterion,[9]

$$C_{W-P} = R_v \cdot R_p^2 / c_s \mathcal{D}_{eff} \quad \text{(S15)}$$

where R_v is the local volumetric reaction rate, R_p is the catalyst pellet radius, c_s is the surface reactant species concentration, and $\mathcal{D}_{eff}$ is the effective mass diffusivity in the catalyst). If $C_{W-P} \ll 1$, intra particle diffusion effects are expected to be negligible, and the use of a catalyst effectiveness factor of unity is appropriate. A typical value of local volumetric CH_4 consumption rate can be determined using the data in Figure 7a: the combined rate of direct SMR and reverse methanation followed by water gas shift is $2\ mol/m^2 - s$ or less for the duration of the reaction step. With a catalyst layer thickness of $1\ mm$ and a mass fraction of $\phi = 0.1$, this corresponds to a volumetric CH_4 consumption rate within the pellet of $R_v = 20\ mol/m^3 - s$. Using a characteristic CH_4 concentration at the surface of $9\ mol/m^3$ (the approximate value of concentration for an ideal gas with a mole fraction of 1/3 at 400°C and $5\ bar$

total pressure) and an effective diffusivity of $6.5 \times 10^{-5}\ m^2/s$, for particles with a maximum radius of $R_p = 0.15\ mm$, the Weisz-Prater parameter is approximately $C_{W-P} \sim 7 \times 10^{-4}$.

S7. Timescale Analysis

The main body of the paper presents the method by which the "representative" mole fractions of the various species inside the reactor are calculated for each timescale regime. This supplementary section clarifies the calculation of the CO_2 mole fraction for the "fast adsorption" regime and supplies additional information on the use of the representative mole fractions to determine the resulting rate of CH_4 consumption ($\bar{r}_{CH_4}$).

S7.1 Average CO_2 Partial Pressure for "Fast" Adsorption

The average CO_2 partial pressure depends on the average CO_2 loading on the sorbent, as the two are linked through the adsorption isotherm. Figure S19 illustrates a representative CO_2 isotherm, with an inflection point due to the chemical complexation reaction. The "carried over" CO_2 loading from the previous cycle (due to incomplete desorption/regeneration) is labeled P_{des}, and the saturation loading (or the highest possible sorbent loading in the limit that $P_{CO_2} \to \infty$) is labeled q_{sat}. For an order-of-magnitude estimation, the average CO_2 loading on the sorbent is taken to be the average of the initial loading (given by the isotherm when CO_2 pressure is P_{des}) and the final loading (assumed to reach saturation loading q_{sat}).

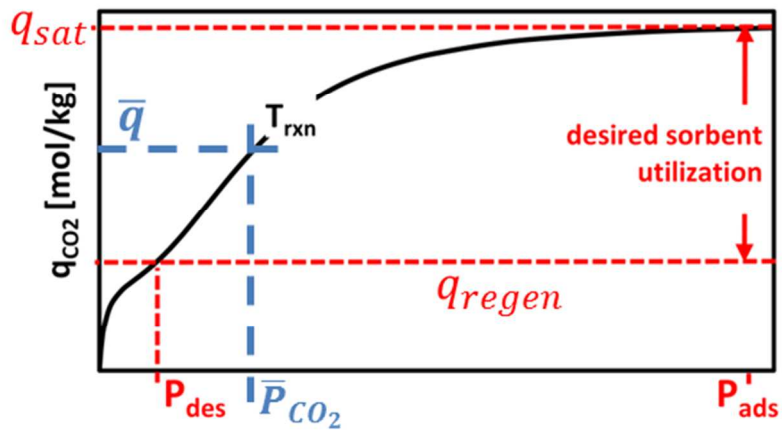

Figure S19: Determination of characteristic sorbent loading ($\bar{q}$) and CO_2 partial pressure ($\bar{P}_{CO_2}$) from the adsorption isotherm.

The corresponding average CO_2 partial pressure ($\bar{P}_{CO_2}$) is then the CO_2 partial pressure at which the adsorption isotherm gives an equilibrium CO_2 loading equal to $\bar{q}$, as specified by eq S13.

S7.2 Determination of Average Fuel Consumption Rate

The rate of fuel (CH_4) consumption must be determined in a different fashion depending on which process (reaction, adsorption or permeation) is limiting its rate of change. For the reaction timescale calculation, the kinetic model shows that the rates of the two parallel paths for H_2 production (reverse methanation followed by water gas shift, or direct steam methane reforming) are of similar magnitude. As such, only the rate of the (direct) steam methane reforming reaction (r_3) is calculated using the kinetic model from Xu and Froment and twice this value is used to determine the molar rate of CH_4 consumption in the reactor:

$$\bar{r}_{CH_4,rxn} = 2\bar{\rho}\phi A_c d_{cat} r_3 \qquad \text{(S16)}$$

For the permeation timescale, the rate of CH_4 consumption is balanced by the rate of H_2 permeation through the membrane. Stoichiometry of the SMR process ($2H_2O + CH_4 \rightleftarrows 4H_2 + CO_2$) dictates that

these will occur in a 4:1 hydrogen to methane ratio. The characteristic CH_4 consumption rate for the permeation timescale calculation is then evaluated as one fourth of the hydrogen permeation rate:

$$\bar{r}_{CH_4,perm} = \frac{1}{4} \cdot A_c \frac{D_{mem}}{\delta} \left[\left(x_{H_2} P_T \right)^{1/2} - P_{H_2}^{\infty\, 1/2} \right] \tag{S17}$$

For the adsorption timescale, the rate of CH_4 consumption is balanced by the rate of CO_2 adsorption. In this case, the stoichiometry of (direct) steam reforming reaction dictates that these will occur in a 1:1 methane to carbon dioxide ratio, *i.e.*,

$$\bar{r}_{CH_4,ads} = \bar{\rho}(1-\phi) A_c d_{cat} k_{ldf} \left[q_{eq}\left(x_{CO_2}, P_T \right) - \bar{q} \right] \tag{S18}$$

For any of the timescale calculations, the appropriate fuel consumption rate (as determined by either eq. S16, S17 or S18) is used, along with the total initial number of moles of fuel ($N_{CH_4}^0$), to estimate the time required to consume all of the initial quantity of fuel.

The initial quantity of fuel (for a given reactor height) will have a slight temperature dependence, as according to the ideal gas equation of state the molar density of a gas is inversely proportional to the reactor temperature T. Additionally, a small quantity of fuel is interspersed in the void volume of the porous bed. From the ideal gas equation of state, the initial number of moles of fuel is $x_{CH_4}^0 P_T A_c (H_0 + \bar{\varepsilon} d_{cat})/R_u T$ and the resulting process timescale is:

$$\tau_{process} = \frac{x_{CH_4}^0 P_T A_c (H_0 + \bar{\varepsilon} d_{cat})/R_u T}{\bar{r}_{CH_4,process}} \tag{S19}$$

It is possible, however, to remove the temperature dependence and correct for the fuel located within the catalyst/sorbent layer by defining an effective initial height as $H_0^{eff} = (H_0 + \bar{\varepsilon} d_{cat}) \cdot T_{ref}/T$. To remain consistent throughout the paper, 400°C is chosen as a reference temperature (as this is the baseline operating temperature for the initial analysis). Substituting the definition for H_0^{eff} into eq S19 yields a non-operating temperature dependent version of "process resistance", or timescale divided by (effective) initial reactor height:

$$resistance = \tau_{process}/H_0^{eff} = \frac{x_{CH_4}^0 P_T A_c / R_u T_{ref}}{\bar{r}_{CH_4,process}} \quad \text{(S20)}$$

The process resistance can be mapped to equivalent H_2 yield rates by recognizing that, with a hydrogen yield efficiency in excess of 99% which is typical for a CHAMP-SORB reactor, essentially 4 moles of H_2 will be produced per initial mole of CH_4 initially in the reactor. Furthermore, because the time to completion, in the limit that all other processes are "fast" relative to the process under consideration, is well represented by the process timescale, the hydrogen yield rate per unit of cross-sectional area is:

$$r''_{H_2,yield} = \frac{4 x_{CH_4}^0 P_T / R_u T_{ref}}{resistance} \quad \text{(S21)}$$

For example, a "resistance" of 10 s/cm will correspond to a hydrogen yield rate per unit area of:

$$r''_{H_2,yield} = \frac{4(1/3)(5\ bar) \Big/ \left(8.314 \times 10^{-5} \frac{m^3 - bar}{mol - K}\right)(673\ K)}{\left(10 \frac{s}{cm}\right) \times (100\ cm/m)} = 0.119\ mol\ H_2/m^2 - s \quad \text{(S22)}$$

The equivalent H_2 yield rates illustrated in Figure 11 of the main paper are calculated in the manner illustrated in eqs S21 and S22.

S8. CHAMP-SORB Cyclic Operation

While this manuscript focuses on the most critical, H_2 producing step of the CHAMP-SORB process, a brief review of the overall cycle and a kinetic study of the sorbent regeneration process is useful for the reader. A more in depth thermodynamic assessment of the entire CHAMP-SORB operating cycle can be found in our previous study.[5]

S8.1 Operation Schematic

Figure S20 illustrates the entire CHAMP-SORB cyclic operation. Proceeding clockwise from top left in Figure S20, the reactor is first filled with a mixture of CH_4 and H_2O, as well as recycled products from the

previous cycle (if desired). The mixture then undergoes the steam-methane reforming reaction, which is enhanced by permeation of H_2 through the palladium-silver membrane and adsorption of CO_2. During this step, the piston moves downward to maintain constant pressure as selected species are removed from the gas phase via adsorption and permeation, and the temperature is maintained by heating (not shown) the sorbent/catalyst mixture layer. After the SMR reaction has proceeded sufficiently, the exhaust valve opens and the downstroke is completed to fully exhaust the chamber. As denoted by the dotted line, part or all of the exhaust gases can be recycled to the filling upstroke of the next CHAMP cycle if losses of residual hydrogen and unconverted methane upon exhaust are to be minimized.

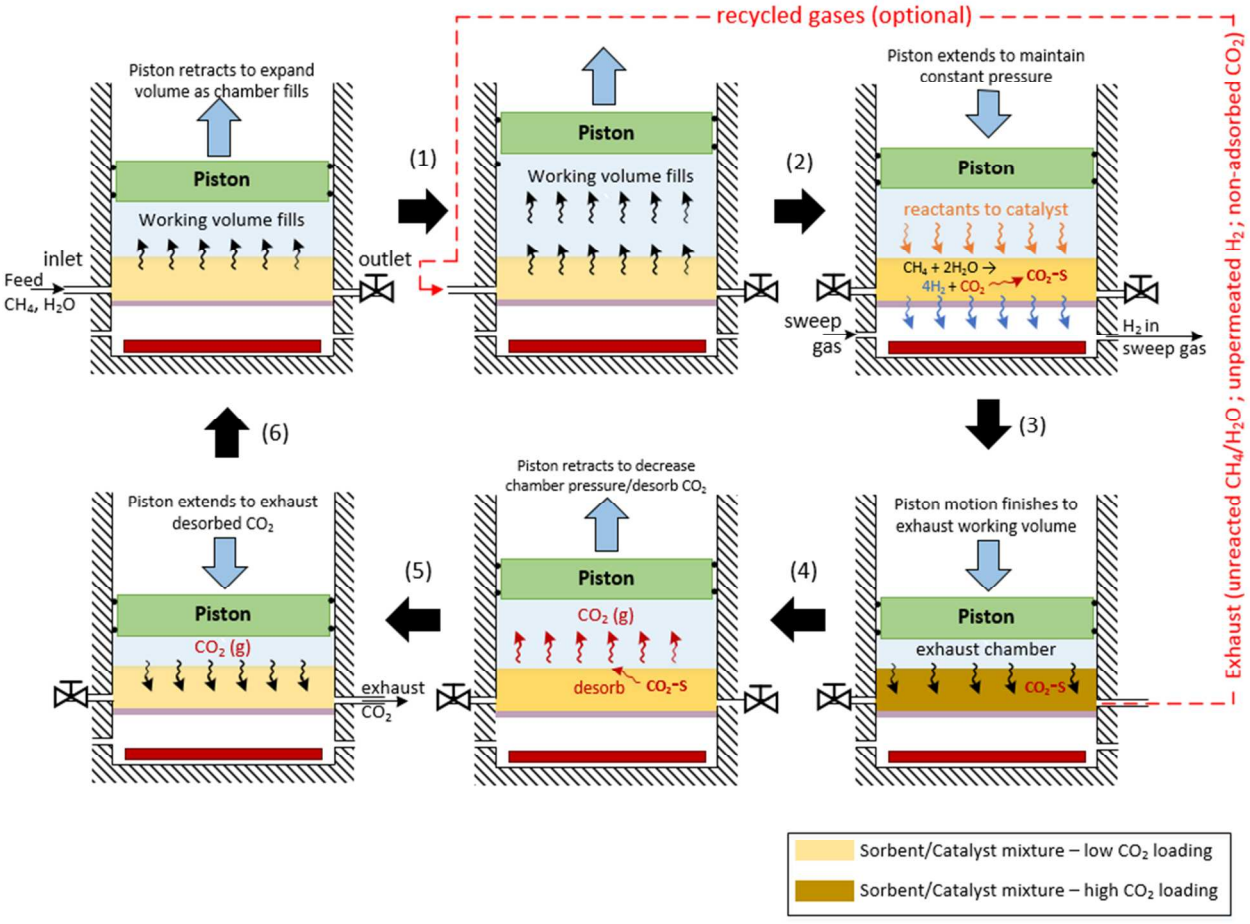

Figure S20: Schematic of CHAMP-SORB reactor cycle. The reactor utilizes four strokes per cycle: (a) retracting piston to fill the reactor, (b) extending piston to produce H_2 via SMR at constant pressure and then opening valve to exhaust products, (c) retracting piston to desorb CO_2 and (d) extending piston to desorb and produce a purified CO_2 as the final product.

S8.2 Kinetic Study of Sorbent Regeneration via Reactor Volume Expansion

The ideal, purely kinetic, model can also be used to assess the ideal reactor behavior during other steps in the CHAMP-SORB cycle, in particular to develop a basic understanding of how the pressure-swing regeneration approach would work in a variable volume reactor. Specifically of interest are two questions:

(i) Is it possible to achieve a substantial sorbent regeneration level of $q_0 = 0.25\ mol/kg$ using pressure swing via volume expansion alone, or would some complementary temperature swing also be necessary?

(ii) What fraction of the total cycle time is taken up by regeneration versus the reaction (H_2 producing) steps, with impact on expected power/hydrogen yield density of the CHAMP-SORB cycle?

To answer these questions, the ideal kinetic model developed in section 4.1 of the main manuscript is employed to study the complete CHAMP-SORB regeneration cycle. The system starts with a reaction step governed by equations (4) – (8), followed by an exhaust step, then volume expansion to produce low pressure conditions favorable for CO_2 desorption and sorbent regeneration, then exhaust of the desorbed CO_2, and finally refilling of the reactor to begin a new cycle. For the exhaust step, the time rate of change of moles in the system decays proportional to a valve coefficient (k_V) and the difference between the total reactor pressure and ambient ($P_T - P_{atm}$),

$$\frac{dN_T}{dt} = -k_V(P_T - P_{atm}) \qquad \text{(S23)}$$

where the reactor pressure is calculated using the ideal gas equation of state, eq (7) in the main manuscript. Following with the ideal assumption of perfect mixing, the mixture composition at the outlet valve must be equal to the bulk composition in the reactor, and the time rate of change in number of moles of each individual species j during the exhaust step is equal to the time rate of change of the total moles in the reactor, given by equation (S23), multiplied by the mole fraction x_j of a given species ($dN_j/dt = x_j \cdot dN_T/dt$).

In modeling the desorption step, the piston is moved away from the catalyst/sorbent bed to expand the reactor volume at a velocity U_{max}^{P} ($dH/dt = U_{max}^{P}$) until it reaches the maximum volume (equal to that at the start of the reaction step), and the pressure varies according to eq (7) of the main manuscript. During desorption step, the inlets/outlets to the reactor are closed and $dN_j/dt = 0$ for all species other than CO_2, which may desorb into the gas volume, as favorable conditions for desorption occur due to pressure drop as the reactor volume expands:

$$\frac{dN_{CO_2}}{dt} = -\overline{\rho} dA_c (1-\phi) \frac{dq_{CO_2}}{dt} \tag{S24}$$

where the time rate of change of CO_2 loading is determined using the linear driving force kinetics (eq (6) of the main manuscript). The desorption step is allowed to continue until the CO_2 loading on the sorbent approaches within 3% of its equilibrium value, at which point the piston begins to move downward to exhaust the desorbed CO_2 from the reactor. Because the pressure in the CHAMP-SORB is likely below atmospheric at the end of the desorption step, the CO_2 exhaust step first consists of a period of time where the piston moves downward at its maximum velocity ($dH/dt = -U_{max}^{P}$) and only CO_2 can begin to re-adsorb onto the sorbent, according to equation (S24), as pressure in the reactor rises. Once atmospheric pressure is reached, the piston continues to move downward at $-U_{max}^{P}$, pushing all species out of the reactor at rates proportional to the mole fraction of each. Before the reactor can be refilled with CH_4 and H_2O to begin the next reaction step, the sorbent loading must reach its initial, periodic quasi-steady state loading value(q_0) for the cycle. If this does not occur after one expansion/desorption followed by CO_2 exhaust step, the process can be repeated until the target sorbent loading is reached.

As a baseline case, conditions matching those of section 4.3 are chosen ($T = 400$℃, $P_T = 5\ bar$, $P_{H_2}^{\infty} = 0.2\ bar$, $q_0 = 0.25\ mol/kg$, $\delta = 50\ \mu m$, $H_0 = 2\ cm$). A catalyst loading of $0.1\ kg/m^2$ is utilized with a sorbent mass of $1.25\ kg/m^2$, a value calculated to ensure that a sufficient amount of CO_2 can be adsorbed to allow the reactor to reach full conversion when starting with a sorbent loading of $0.25\ mol/kg$. A valve coefficient of $0.004\ mol/bar-s$ is chosen such that the reactor

depressurization during the first exhaust step takes $\sim 5\ s$, and a moderate piston velocity of $U_{max}^{P} = 3\ cm/s$ is utilized for the CO_2 desorption and exhaust steps. Figure S21 illustrates the transient rate of H_2 yield, reactor chamber extent (piston position), pressure and sorbent loading for 3 consecutive cycles.

In Figure S21, the H_2 production step lasts for approximately $500\ s$, with the CHAMP-SORB reactor sustaining elevated H_2 production rates until the piston can no longer provide compression (when the height reaches zero and the piston comes in contact with the packed bed, just after $t = 500\ s$). At this point, the reactor is first depressurized according to equation (S23), then the piston moves upward to expand the reactor volume and create favorable conditions for CO_2 desorption. During this step, the reactor pressure first drops well below atmospheric level, but then begins to recover as CO_2 desorbs from the sorbent and enters the reaction chamber. When a pressure of approximately $0.6\ bar$ is reached, the sorbent is near equilibrium with the gas-phase CO_2 and the CO_2 exhaust step begins, during which the reactor is first compressed to atmospheric pressure and then CO_2 begins exiting the reactor chamber.

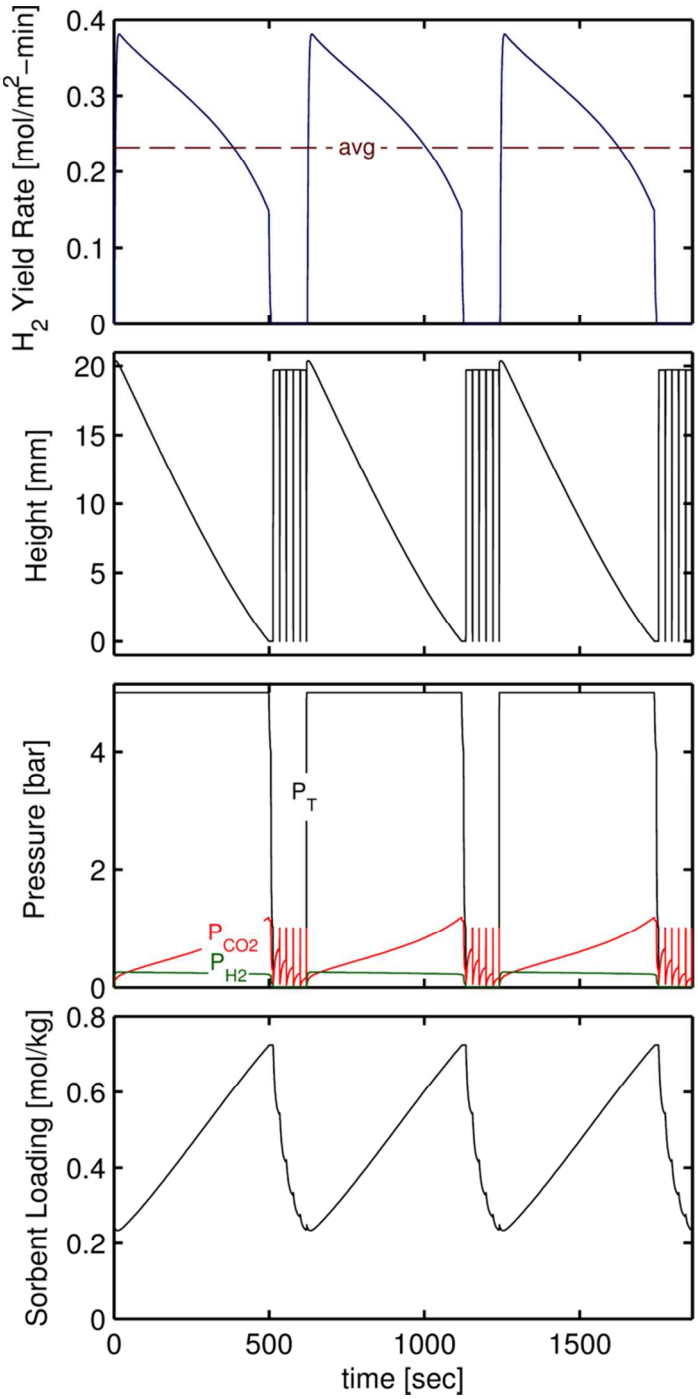

Figure S21: Time varying H_2 yield rate, reactor height, reactor pressure, and sorbent loading for three consecutive cycles of CHAMP-SORB operation with volume-expansion driven pressure-swing desorption. Five volume expansions are required to restore the CO_2 sorbent loading to its initial value, when the reactor is ready to start a new reaction cycle.

During the first CO_2 desorption step, the sorbent loading drops from a maximum value of $0.73\ mol/kg$ at the end of the reaction step to roughly $0.5\ mol/kg$ after completion of volume expansion and CO_2 desorption. In order to fully regenerate the sorbent to the $q_0 = 0.25\ mol/kg$ initial loading value, five repetitions of volume expansion step of CO_2 desorption followed by CO_2 exhaust are required with each successive step reducing the CO_2 loading further. The time required for this desorption, however is only approximately $110\ s$ out of the total $620\ s$ cycle time, or roughly 18% of the cycle time is spent exhausting and regenerating the reactor. The impact of sorbent regeneration on average H_2 production rate is illustrated in the top plot of Figure S21.

Figure S22 illustrates the piston position (reactor volume/height), pressure and sorbent loading for just the first desorption step, showing data from $500 \leq t \leq 550\ s$ in Figure S21. Here, the initial (first) exhaust step in the sequence, between the dotted vertical lines marked (1) and (2), can be clearly seen, followed by the volume expansion and subsequent CO_2 desorption (noted by a rise in reactor CO_2 partial pressure and drop in sorbent loading) that occurs between the lines marked (2) and (3).

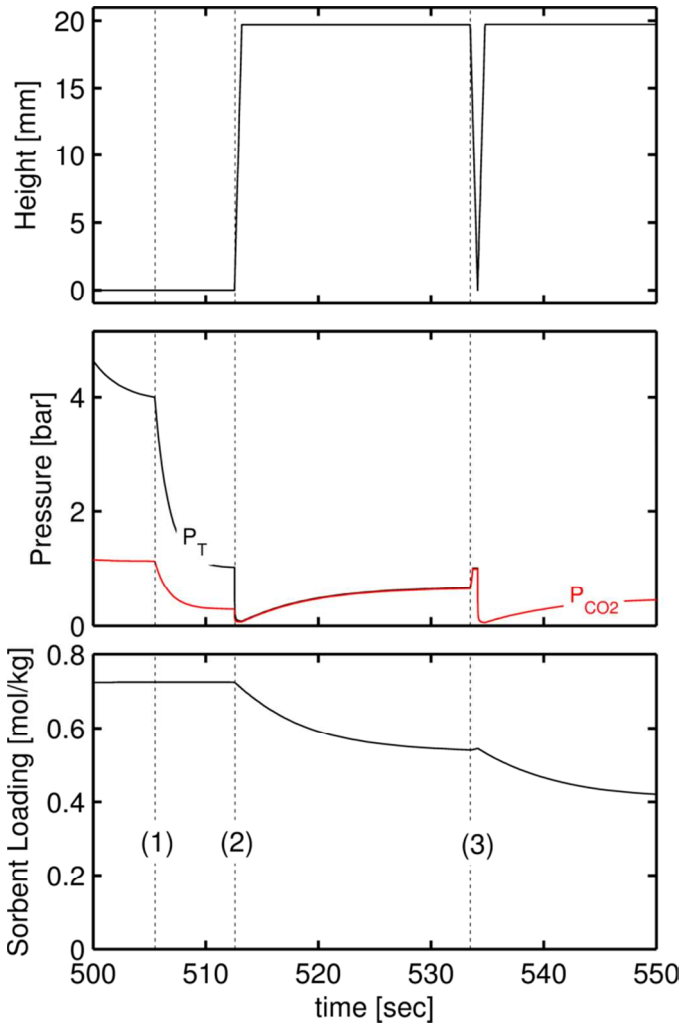

Figure S22: Time varying reactor height, reactor pressure, and sorbent loading for a single volume-expansion driven pressure-swing desorption step with a piston velocity of $3\ cm/s$.

The sorbent loading rises slightly just after the time instant marked (3), due to re-adsorption of CO_2 as the reactor is recompressed to atmospheric pressure to allow it to be exhausted, however the exhaust process is sufficiently quick relative to the adsorption timescale that a substantially quantity of CO_2 is not reloaded on the sorbent. A piston velocity of $3\ cm/s$ is selected for volume expansion such that roughly $1\ s$ is required for the piston to travel the height of the reactor, a time sufficiently short to avoid significant desorption during the exhausting step (as predicted by the adsorption timescale of $1/k_{ldf} \sim 20\ s$).

While the analysis of this section shows that it is possible to regenerate the sorbent to a level of $q_0 = 0.25\ mol/kg$ using purely volume-expansion driven pressure swing adsorption, and that the time required to reach this value is less than 20% of the total cycle time, it may be desired to incorporate some temperature swing to minimize the number of expansion steps required to reach a suitable sorbent regeneration level without exposing the thin, hydrogen-permeable membrane to many pressure cycles, which may negatively impact its life time and reactor reliability. These simulations, conducted using an idealized kinetic model, neglect the mass transfer effect of CO_2 through the packed bed as well as any thermal effects. Mass transport is expected to be less significant in this part of the operating cycle (as compared to the combined reaction/permeation/adsorption step) because CO_2 is essentially the only species contained in the reactor and it is assumed that the CO_2 pressure will equilibrate via advection on the sonic timescale in the reactor. As such, the conclusions presented in this section are a good first pass at assessing the regeneration, and future work could account for all of these factors in a rigorous fashion to obtained refined predictions.

S9. Energy Considerations: Variable Volume Compression Work and Exergy of Heat Input

Because the CHAMP-SORB adds the requirement of high-level mechanical work input for variable volume operation that is not present in the standard SMR process, it is important to understand the magnitude of this work required relative to (*i*) the endothermic heat of reaction and (*ii*) the useful energy carried by the H_2 produced by the reaction. For the simulation reported in section 4.3 (Figures 6 and 7) with a catalyst mass fraction of $\phi = 0.1$, a reactor of 1 m^2 cross-sectional area and initial height 0.02 m at 400°C will initially contain $N_{CH_4}^0 = 0.603\ mol$ of methane fuel. The required endothermic heat of the overall SMR reaction is $\Delta H_{rxn} = 164.9 \frac{kJ}{mol}$(according to eq 3), and as essentially 100% of the

fuel is converted the required heat input during a single reaction step is $Q_{in} = N^0_{CH_4}\Delta H_{rxn} = 99.4\ kJ$. For comparison, considering isobaric compression over the full height of the reactor, the ideal work of compression is $W_{in} = P\Delta V = (5\ bar)(0.02\ m^3)(100\ kJ/bar - m^3) = 10\ kJ$ (assuming the process is adiabatic and reversible with negligible frictional losses). From the above calculations, the ideal mechanical work is approximately **10%** of the minimum heat input for reaction – in reality this number will be larger due to frictional losses; however the piston velocity is relatively slow (moving 2 cm over several minutes), indicating that frictional losses may not play a substantial role in the calculation. If one wishes to consider the exergetic efficiency of the compression process, accounting for the fact that a greater amount of heat input would be needed to produce a given amount of work (*i.e.,* work is more directly valuable than heat), the work to heat ratio can be multiplied by a factor of $(1 - T_{amb}/T_{rxn})^{-1}$. For a reaction temperature of $T_{rxn} = 400$℃ relative to an ambient temperature of $T_{amb} = 25$℃, the exergetic adjusted ratio of compression work to reaction heat input is **18%** (or $10\% \times (1 - 298K/673K)^{-1}$).

While this exergetic analysis is certainly instructive in assessing the true thermodynamic cost of the work input required for variable volume operation relative to the required heat input for the endothermic reaction, in practice the electrical energy input for producing the required mechanical work is readily available from other, much high efficiency centralized power sources, including renewable non-thermal routes (e.g., photovoltaics), thus mitigating the negative impact of inclusion thermal-to-electrical/mechanical energy conversion losses. Furthermore, exergetic considerations can also be applied to the required endothermic heat of reaction to show that there is substantial value in providing the heat of reaction at a lower temperature. As calculated above, the required endothermic heat input for the simulation of section 4.3 is $Q_{in} = 99.4\ kJ$. Considering exergy, this amount of heat input could alternatively be used to create an equivalent amount of work which will vary according to temperature at which the heat is supplied and the ambient temperature, $W_{equiv} = Q_{in} \times (1 -$

T_{amb}/T_{rxn}). For the proposed CHAMP-SORB process, the reaction temperature is 400°C, while in comparison the typical SMR process occurs at approximately 900°C. As such, the equivalent work (which is a representation of the true "value" of the heat input, accounting for the difference in quality of heat input based on the temperature at which it is supplied) is only $55.4\ kJ$ for the lower temperature CHAMP-SORB process as compared to $74.1\ kJ$ for the standard SMR process (as the same quantity of heat has higher value at 900°C vs. 400°C). This difference in exergy associated with different temperatures of heat application ($18.7\ kJ$) is actually **greater** than the $10\ kJ$ of required compression work input, indicating that the CHAMP-SORB may actually require less exergy to operate than the standard SMR process. For practical purposes, the standard SMR process will likely require even more energy/exergy input accounting for the fact that heat losses to the environment will be greater when the reactor is held at the much higher temperature required for standard SMR.

Also of interest is a comparison between the required mechanical work input and the lower heating value of the H_2 produced by the reactor. The batch of $N^0_{CH_4} = 0.603\ mol$ of fuel produces $N_{H_2.perm} \sim 2.4\ mol$ of hydrogen, which has a LHV of $242\ kJ/mol$, meaning that the useful energy that can be extracted from the product is $E_{H_2} = LHV_{H_2} \times N_{H_2,perm} = 580\ kJ$. The required mechanical work input is therefore **less than 2%** of the energy carried by the H_2 product produced by the reaction.

References

(1) McLeod, L.; Degertekin, F.; Fedorov, A. Effect of Microstructure on Hydrogen Permeation through Thermally Stable, Sputtered Palladium-Silver Alloy Membranes. *Appl. Phys. Lett.* **2007,** *90*, 261905.

(2) Dormand, J. R.; Prince, P. J. A Family of Embedded Runge-Kutta Formulae. *Journal of Computational and Applied Mathematics* **1980,** *6*, 19.

(3) Walspurger, S.; Boels, L.; Cobden, P. D.; Elzinga, G. D.; Haije, W. G.; van den Brink, R. W. The Crucial Role of the K+–Aluminium Oxide Interaction in K+-Promoted Alumina-and Hydrotalcite-Based Materials for Co2 Sorption at High Temperatures. *ChemSusChem* **2008,** *1*, 643.

(4) Lee, K. B.; Verdooren, A.; Caram, H. S.; Sircar, S. Chemisorption of Carbon Dioxide on Potassium-Carbonate-Promoted Hydrotalcite. *J. Colloid. Interf. Sci.* **2007,** *308*, 30.

(5) Anderson, D. M.; Kottke, P. A.; Fedorov, A. G. Thermodynamic Analysis of Hydrogen Production Via Sorption-Enhanced Steam Methane Reforming in a New Class of Variable Volume Batch-Membrane Reactor. *Int. J. Hydrogen Energy* **2014,** *39*, 17985.

(6) Sircar, S.; Hufton, J. R. Why Does the Linear Driving Force Model for Adsorption Kinetics Work ? *Adsorption* **2000,** *6*, 137.

(7) Lee, K. B.; Beaver, M. G.; Caram, H. S.; Sircar, S. Reversible Chemisorbents for Carbon Dioxide and Their Potential Applications. *Ind. Eng. Chem. Res.* **2008,** *47*.

(8) Xu, J. G.; Froment, G. F. Methane Steam Reforming, Methanation and Water-Gas Shift 1. Intrinsic Kinetics. *AIChE J.* **1989,** *35*, 88.

(9) Weisz, P.; Prater, C. Interpretation of Measurements in Experimental Catalysis. *Adv. Catal.* **1954,** *6*, 143.